Inorg. Chem. **2006**, *45*, 609–626

Aggregation of [(^{t}Bu$_3$SiS)MX]: Structures of {[Br$_2$Fe(μ-SSi^{t}Bu$_3$)$_2$FeBr(THF)]Na(THF)$_4$}$_\infty$, *cis*-[(THF)FeI]$_2$(μ-SSi^{t}Bu$_3$)$_2$, [(^{t}Bu$_3$SiS)Fe]$_2$(μ-SSi^{t}Bu$_3$)$_2$, and Comparative Structure and Magnetism Studies of [(^{t}Bu$_3$SiS)MX]$_n$ (M = Fe, Co, X = Cl, n = 12; M = Fe, Ni, X = Br, n = 12; M = Fe, X = I, n = 14)

Orson L. Sydora,[†] Thomas P. Henry, Peter T. Wolczanski,*[,†] Emil B. Lobkovsky,[†] Evan Rumberger,[‡] and David N. Hendrickson*[,‡]

Department of Chemistry and Chemical Biology, Baker Laboratory, Cornell University, Ithaca, New York 14853, and Department of Chemistry and Biochemistry, University of California, San Diego, California 92083

Received July 29, 2005

A convenient synthesis of ^{t}Bu$_3$SiSH and ^{t}Bu$_3$SiSNa(THF)$_x$ led to the exploration of "^{t}Bu$_3$SiSMX" aggregation. The dimer, [(^{t}Bu$_3$SiS)Fe]$_2$(μ-SSi^{t}Bu$_3$)$_2$ (**1**$_2$), was formed from [{(Me$_3$Si)$_2$N}Fe]$_2$(μ-N(SiMe$_3$)$_2$)$_2$ and the thiol, and its dissolution in THF generated (^{t}Bu$_3$SiS)$_2$Fe(THF)$_2$ (**1**–(THF)$_2$). Metathetical procedures with the thiolate yielded aggregate precursors [X$_2$Fe](μ-SSi^{t}Bu$_3$)[FeX(THF)]Na(THF)$_4$ (**3**–X, X = Cl, Br) and *cis*-[(THF)IFe]$_2$(μ-SSi^{t}Bu$_3$)$_2$ (**4**). Thermal desolvations of **3**–Cl, **3**–Br and **4** afforded molecular wheels [Fe(μ-X)(μ-SSi^{t}Bu$_3$)]$_{12}$(C$_6$H$_6$)$_n$ (**5**–FeX, X = Cl, Br) and the ellipse [Fe(μ-I)(μ-SSi^{t}Bu$_3$)]$_{14}$(C$_6$H$_6$)$_n$ (**6**–FeI). Related metathesis and desolvation sequences led to wheels [Co(μ-Cl)(μ-SSi^{t}Bu$_3$)]$_{12}$(C$_6$H$_6$)$_n$ (**5**–CoCl) and [Ni(μ-Br)(μ-SSi^{t}Bu$_3$)]$_{12}$(C$_6$H$_6$)$_n$ (**5**–NiBr). The nickel wheel disproportionated to give, in part, [(^{t}Bu$_3$SiS)Ni]$_2$(μ-SSi^{t}Bu$_3$)$_2$ (**7**), which was also synthesized via salt metathesis. X-ray structural studies of **1**$_2$ revealed a roughly planar Fe$_2$S$_4$ core, while **1**–(THF)$_2$, **3**–Br, and **4** possessed simple distorted tetrahedral and edge-shared tetrahedral structures. X-ray structural studies revealed **5**–MX (MX = FeCl, FeBr, CoCl, NiBr) to be wheels based on edge-shared tetrahedra, but while the pseudo-D_{6d} wheels of **5**–FeCl, **5**–CoCl, and **5**–FeBr pack in a body-centered arrangement, those of pseudo-C_{6v} **5**–NiBr exhibit hexagonal packing and two distinct trans-annular *d*(Br···Br). Variable-temperature magnetic susceptibility measurements were conducted on **5**–FeCl, **5**–CoCl, **5**–FeBr, and **6**–FeI, and the latter three are best construed as weakly antiferromagnetic, while **5**–FeCl exhibited modest ferromagnetic coupling. Features suggesting molecular magnetism are most likely affiliated with phase changes at low temperatures.

Introduction

The aggregation of low-coordinate transition metal complexes can lead to a fascinating array of oligomers, polymers, or clusters depending on the nature of the bridging ligands. Tetrahedral species are often desirable building blocks for extended arrays;[1−3] hence, XMY equivalents were sought for aggregation to [M(μ-X)(μ-Y)]$_n$, which were expected to be oligomeric or polymeric on the basis of the *edge* connectivity intrinsic to tetrahedra. Literature precedent[4] for thiolate bridging groups in the development of nitrogenase-related cluster chemistry of iron and other first-row transition metals suggested that ^{t}Bu$_3$SiS$^-$ would be a valuable ligand. In addition, its solubility properties would permit synthetic studies to be carried out in nonpolar, aprotic media, and its steric features would help ensure low coordination, as investigations with the related siloxide, ^{t}Bu$_3$SiO$^-$ (silox),[5] had already shown. Herein, we report the aggregation of

* To whom correspondence should be addressed. E-mail: ptw2@cornell.edu (P.T.W.); dhendrickson@ucsd.edu (D.N.H.).
[†] Cornell University.
[‡] University of California, San Diego.

(1) Zheng, C.; Hoffmann, R.; Nelson, D. R. *J. Am. Chem. Soc.* **1990**, *112*, 3784−3791.
(2) Hartl, H.; Mahdjour-Hassan-Abadi, F. *Angew. Chem., Int. Ed. Engl.* **1994**, *33*, 1841−1842.
(3) Férey, G. *Angew. Chem., Int. Ed.* **2003**, *42*, 2576−2579.
(4) Dance, I. G. *Polyhedron* **1986**, *5*, 1037−1104.

10.1021/ic051289u CCC: $33.50
Published on Web 12/24/2005

[(^{t}Bu$_3$SiS)MX] (X = halide) to cyclic oligomers, studies of their precursors, and some unusual magnetic properties of these compounds. The structures of several cyclics have been previously communicated.[6,7]

Results

1. Thiolate Synthesis. The original multistep synthesis of ^{t}Bu$_3$SiSH (eq 1−4), developed separately by Wiberg[8] and Henry,[9] consisted of the sodium metal reduction of ^{t}Bu$_3$SiBr in THF to afford the supersilanide ^{t}Bu$_3$SiNa(THF)$_2$[10] in 98% yield followed by double nucleophilic substitution of sulfur monochloride to produce ^{t}Bu$_3$Si−SS−Si^{t}Bu$_3$ (74%). Subsequent reduction of the disulfide with 0.9% Na/Hg in THF generated the thiolate ^{t}Bu$_3$SiSNa(THF)$_x$ (x = 1.4−1.9), but with inconsistent yields (∼55%). The sodium thiolate was protonated with anhydrous HCl and purified by sublimation, yielding the thiol ^{t}Bu$_3$SiSH (84%). LiAlH$_4$ proved to be a superior reducing agent, which, upon acidic workup and sublimation, afforded the thiol in 83% yield (eq 5).

$$^t\text{Bu}_3\text{SiBr} + 2\ \text{Na}^0 \xrightarrow[\Delta,\ 12\ \text{h}]{\text{THF}} {}^t\text{Bu}_3\text{SiNa(THF)}_2 + \text{NaBr} \quad (1)$$

$$2\,{}^t\text{Bu}_3\text{SiNa(THF)}_2 + \text{Cl−SS−Cl} \xrightarrow[-78\ ^\circ\text{C}]{\text{THF}} {}^t\text{Bu}_3\text{Si−SS−Si}{}^t\text{Bu}_3 + 2\text{NaCl} \quad (2)$$

$$^t\text{Bu}_3\text{Si−SS−Si}{}^t\text{Bu}_3 + 2\text{Na/Hg} \xrightarrow[23\ ^\circ\text{C},\ 3\ \text{d}]{\text{THF}} 2\,{}^t\text{Bu}_3\text{SiSNa(THF)}_x \quad (3)$$

$$^t\text{Bu}_3\text{SiSNa(THF)}_x + \text{HCl} \xrightarrow[23\ ^\circ\text{C},\ 30\ \text{min}]{\text{THF}} {}^t\text{Bu}_3\text{SiSH} + \text{NaCl} \quad (4)$$

$$^t\text{Bu}_3\text{Si−SS−Si}{}^t\text{Bu}_3 + \text{LiAlH}_4\ (\text{excess}) \xrightarrow[2)\ \text{H}_2\text{O, HCl (aq)}]{1)\ \text{THF, }\Delta\text{, 2 d}} 2\,{}^t\text{Bu}_3\text{SiSH} \quad (5)$$

This rather tedious sequence was shortened considerably when Wiberg reported that the triflate, ^{t}Bu$_3$SiOTf,[11] could be substituted with anhydrous sodium hydrogensulfide upon reluxing in THF (eq 6), whereas substitution of ^{t}Bu$_3$SiBr did not occur. Care must be taken to use rigorously anhydrous NaSH or

$$^t\text{Bu}_3\text{SiOTf} + \text{NaSH} \xrightarrow[\Delta,\ 5\ \text{d}]{\text{THF}} {}^t\text{Bu}_3\text{SiSH} + \text{NaOTf} \quad (6)$$

$$^t\text{Bu}_3\text{SiSH} + \text{Na°}\ (\text{excess}) \xrightarrow[\Delta,\ 12\ \text{h}]{\text{THF}} {}^t\text{Bu}_3\text{SiSNa(THF)}_x + {}^1/_2\text{H}_2 \quad (7)$$

^{t}Bu$_3$SiOH forms instead of the thiol. ^{t}Bu$_3$SiSH was deprotonated with sodium metal in THF to give the corresponding sodium thiolate, ^{t}Bu$_3$SiSNa(THF)$_x$, in 92% yield (eq 7). Overall, the two step synthesis yields ^{t}Bu$_3$SiSH in 6 d with a 66% yield from ^{t}BuSiH (addition of triflic acid yields ^{t}Bu$_3$SiOTf (78%)),[11] while the original multistep route takes 8 d and provides thiol in 34% yield from ^{t}Bu$_3$SiH.

2. The Dimer, [(^{t}Bu$_3$SiS)Fe]$_2$(μ-SSi^{t}Bu$_3$)$_2$. 2.1. Synthesis and Reactivity. Treatment of [(Me$_3$Si)$_2$N]$_2$Fe[12] with 4 equiv of ^{t}Bu$_3$SiSH afforded orange crystalline [(^{t}Bu$_3$SiS)Fe]$_2$-(μ-SSi^{t}Bu$_3$)$_2$ (**1**$_2$) in 86% yield according to eq 8. ^{1}H NMR spectra of **1**$_2$ in benzene-d_6 revealed two broad resonances at

$$2[(\text{Me}_3\text{Si})_2\text{N}]_2\text{Fe} + 4\,{}^t\text{Bu}_3\text{SiSH} \xrightarrow[23\ ^\circ\text{C},\ 30\ \text{min}]{\text{C}_6\text{H}_6} \underset{\mathbf{1}_2}{[({}^t\text{Bu}_3\text{SiS})\text{Fe}]_2(\mu\text{-SSi}{}^t\text{Bu}_3)_2} + 4(\text{Me}_3\text{Si})_2\text{NH} \quad (8)$$

$$\mathbf{1}_2 \xrightarrow[23^\circ\text{C}]{\text{THF}} \underset{\mathbf{1}\text{−(THF)}_2}{2({}^t\text{Bu}_3\text{SiS})_2\text{Fe(THF)}_2} \quad (9)$$

$$2(\underset{\mathbf{2}\text{−THF}}{{}^t\text{Bu}_3\text{SiS})_3\text{Fe(THF)}} \xrightarrow[23\ ^\circ\text{C},\ 3\ \text{wk}]{\text{hexane/Me}_3\text{SiOSiMe}_3} \mathbf{1}_2 + {}^t\text{Bu}_3\text{Si−SS−Si}{}^t\text{Bu}_3 + 2\text{THF} \quad (10)$$

$$\text{FeCl}_3\text{(THF)} + 3\,{}^t\text{Bu}_3\text{SiSNa(THF)}_x \xrightarrow[23\ ^\circ\text{C},\ 6\ \text{h}]{\text{THF}} \underset{\mathbf{2}\text{−THF}}{({}^t\text{Bu}_3\text{SiS})_3\text{Fe(THF)}} + 3\ \text{NaCl} \quad (11)$$

δ 1.91 ($\nu_{1/2} \approx$ 200 Hz) and 2.63 ($\nu_{1/2} \approx$ 200 Hz) that correspond to the different thiolates. Addition of 2 equiv of ^{t}Bu$_3$SiSNa to **1**$_2$ failed to elicit the desired tris-[(^{t}Bu$_3$SiS)$_3$Fe]-Na(THF)$_x$ complex[13] and led to decomposition. In THF, **1**$_2$ was cleaved to afford (^{t}Bu$_3$SiS)$_2$Fe(THF)$_2$ (**1**−(THF)$_2$, 46% isolated yield, eq 9), whose ^{1}H NMR spectrum showed resonances attributable to the thiolate δ 2.84 ($\nu_{1/2} \approx$ 40 Hz) and THF (δ 1.87 ($\nu_{1/2} \approx$ 30 Hz), 4.68 ($\nu_{1/2} \approx$ 80 Hz)) ligands. Dimer **1**$_2$ could be generated concomitant with disulfide from (^{t}Bu$_3$SiS)$_3$Fe(THF) (**2**−THF) in hexane/Me$_3$SiOSiMe$_3$ after a 3 week period at 23 °C (eq 10). The purple ferric thiolate **2**−THF was prepared from FeCl$_3$ and ^{t}Bu$_3$SiSNa in 85% yield (eq 11) and exhibited a single broad resonance in its ^{1}H NMR spectrum at δ 21.4 ($\nu_{1/2} \approx$ 1100 Hz). It degraded to **1**−(THF)$_2$ over the course of a week in THF but much more rapidly if heated or photolyzed.

2.2. Structure of [(^{t}Bu$_3$SiS)Fe]$_2$(μ-SSi^{t}Bu$_3$)$_2$ (1$_2$). Table 1 gives the appropriate data acquisition and refinement parameters for the X-ray structure determination of the dimer, [(^{t}Bu$_3$SiS)Fe]$_2$(μ-SSi^{t}Bu$_3$)$_2$ (**1**$_2$), and Table 2 gives some pertinent interatomic distances and angles. As Figure 1 reveals, **1**$_2$ has essentially a planar Fe$_2$(μ-S)$_2$ diamond

(5) (a) Sydora, O. L.; Wolczanski, P. T.; Lobkovsky, E. B.; Buda, C.; Cundari, T. R. *Inorg. Chem.* **2005**, *44*, 2606−2618. (b) Veige, A. S.; Slaughter, L. M.; Lobkovsky, E. B.; Wolczanski, P. T.; Matsunaga, N.; Decker, S. A.; Cundari, T. R. *Inorg. Chem.* **2003**, *42*, 6204−6224.
(6) Sydora, O. L.; Wolczanski, P. T.; Lobkovsky, E. B. *Angew. Chem., Int. Ed.* **2003**, *42*, 2685−2687.
(7) Sydora, O. L.; Wolczanski, P. T.; Lobkovsky, E. B.; Rumberger, E.; Hendrickson, D. N. *Chem. Commun.* **2004**, 650−651.
(8) Wiberg, N. *Coord. Chem. Rev.* **1997**, *163*, 217−252.
(9) Henry, T. P.; Wolczanski, P. T., unpublished results.
(10) Wiberg, N.; Amelunxen, K.; Lerner, H.-W.; Schuster, H.; Nöth, H.; Krossing, I.; Schmidt-Amelunxen, M.; Seifert, T. *J. Organomet. Chem.* **1997**, *542*, 1−18.
(11) Wiberg, N.; Schuster, H. *Chem. Ber.* **1991**, *124*, 93−95.
(12) Andersen, R. A.; Faegri, K. Jr.; Green, J. C.; Haaland, A.; Lappert, M. F.; Leung, W.-P.; Rypal, K. *Inorg. Chem.* **1988**, *27*, 1782−1786.
(13) MacDonnell, F. M.; Ruhlandt-Senge, K.; Ellison, J. J.; Holm, R. H.; Power, P. P. *Inorg. Chem.* **1995**, *34*, 1815−1822.

Table 1. Crystallographic Data for $[(^tBu_3SiS)Fe]_2(\mu\text{-}SSi^tBu_3)_2$ (**1**$_2$), $(^tBu_3SiS)_2Fe(THF)_2$ (**1**−(THF)$_2$, $[Br_2Fe](\mu\text{-}SSi^tBu_3)_2[FeBr(THF)]Na(THF)_4$ (**3**−Br)

	1$_2$	**1**−(THF)$_2$	**3**−Br	4
formula	$C_{24}H_{54}FeS_2Si_2$	$C_{32}H_{70}FeO_2S_2Si_2$	$C_{44}H_{94}O_5NaSi_2S_2Br_3Fe_2$	$C_{32}H_{70}O_2Si_2S_2I_2Fe_2$
fw	518.84	663.05	1197.93	972.70
space group	*Pbcn*	$P\bar{1}$	$P2_1/c$	$Pna2_1$
Z	8	2	4	4
a, Å	19.382(4)	12.897(2)	24.363(2)	31.884(6)
b, Å	17.872(4)	13.2170(10	13.3296(10)	9.0048(16)
c, Å	17.842(4)	13.2200(10)	17.8294(10)	15.318(3)
α, deg	90	98.100	90	90
β, deg	90	104.320(10)	90.000(2)	90
γ, deg	90	109.860(10)	90	90
V, Å^3	6180.4(23)	1990.1(4)	5790.0(8)	4398.0(14)
ρ_{calc}, g·cm^{-3}	1.115	1.106	1.374	1.469
μ, mm^{-1}	0.710	0.568	2.729	2.237
temp, K	293(2)	293(2)	173(2)	173(2)
λ (Å)	0.71073	0.71073	0.71073	0.71073
R ind [$I > 2\sigma(I)$][a,b]	R1 = 0.0633	R1 = 0.0494	R1 = 0.1103	R1 = 0.0460
	wR2 = 0.1602	wR2 = 0.1311	wR2 = 0.2532	wR2 = 0.1202
R ind (all data)[a,b]			R1 = 0.1109	R1 = 0.0479
			wR2 = 0.2572	wR2 = 0.1211
GOF[c]	1.056	0.991	1.197	1.167

[a] $R1 = \sum||F_o| - |F_c||/\sum|F_o|$. [b] $wR2 = [\sum w(|F_o| - |F_c|)^2/\sum wF_o^2]^{1/2}$. [c] GOF (all data) $= [\sum w(|F_o| - |F_c|)^2/(n - p)]^{1/2}$, n = number of independent reflections, p = number of parameters.

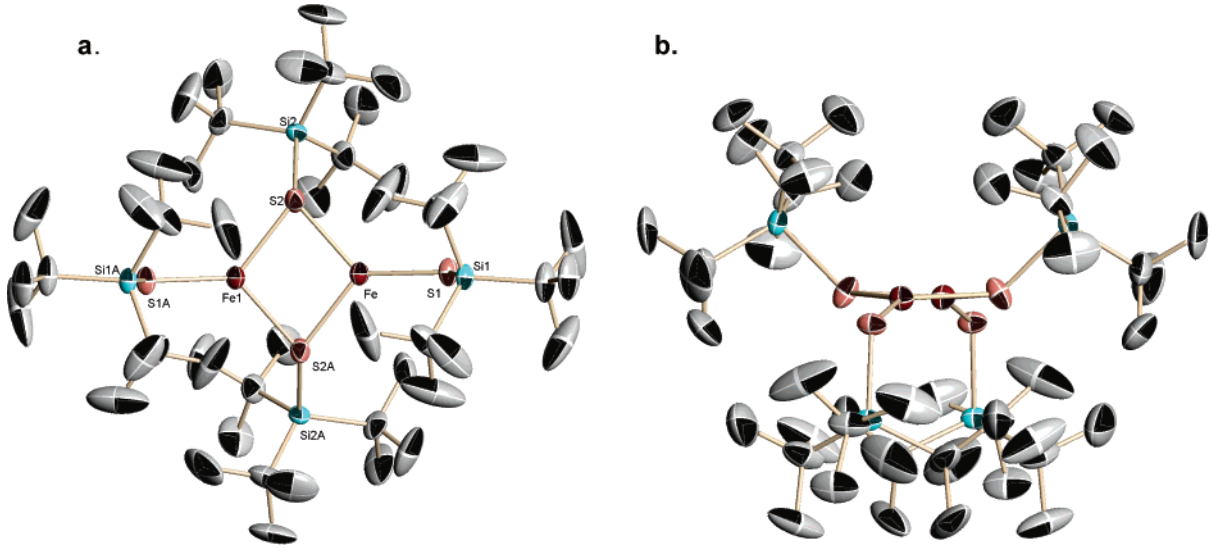

Figure 1. Molecular views of $[(^tBu_3SiS)Fe]_2(\mu\text{-}SSi^tBu_3)_2$ (**1**$_2$): top (a) and side (b).

core,[13−15] with 2.323(2) and 2.333(2) Å iron−sulfur distances, a d(Fe···Fe) of 2.982(2) Å, and Fe−S−Fe and S−Fe−S angles of 79.64(7)° and 100.11(7)°, respectively. The terminal thiolate possesses a slightly shorter iron−sulfur distance of 2.218(2) Å, and its sulfur is positioned slightly "below" the core (S1−Fe−S2/2a = 128.65(8)°/129.62°) while the corresponding ^{t}Bu$_3$Si group is angled (Fe−S1−Si1 = 115.79(9)°) further below. The ^{t}Bu$_3$Si group of the bridging thiolate is positioned "above" the core (Fe1/1a−S2−Si2 = 123.80(10)°/127.37(10)°, as steric influences dictate C_{2v} symmetry.

2.3. Structure of $(^tBu_3SiS)_2Fe(THF)_2$ (1−(THF)$_2$). Difficulties in assigning a structure based on broad NMR spectra led to the X-ray structural characterization of $(^tBu_3SiS)_2Fe(THF)_2$ (**1**-(THF)$_2$), whose data and refinement information is given in Table 1. Table 2 lists selected metric parameters, and the complex is illustrated in Figure 2. **1**-(THF)$_2$ possesses 2.2711(12) and 2.2885(11) Å iron−sulfur distances, and 2.094(3) and 2.136(3) Å iron−oxygen bond lengths. The thiolates are significantly splayed away from each other, as the S1−Fe−S2 angle of 137.33(5)° attests, while the O−Fe−O angle is 86.83(12)°, and the remaining O−Fe−S angles are 100.72(9)°, 102.74(8)°, 104.53(8)° and 113.00(9)°. Overall the molecule is a distorted tetrahedral species, with the ^{t}Bu$_3$Si groups twisted away from one another (Fe−S−Si = 121.07(8)°, 125.33(6)°) to give the molecule approximate C_2 symmetry.

3. Cyclic Oligomer Precursors. 3.1. $[X_2Fe](\mu\text{-}SSi^tBu_3)_2[FeX(THF)]Na(THF)_4$ (3−X, X = Cl, Br). Since the presence of two ^{t}Bu$_3$SiS groups was enough to hamper oligomerization, one thiolate was replaced in order to foment aggregation. A mixture of $FeBr_2(THF)_2$ and ^{t}Bu$_3$SiSNa(THF)$_x$ was stirred in THF for 18−24 h at 23 °C to afford

(14) Power, P. P.; Shoner, S. C. *Angew. Chem., Int. Ed. Engl.* **1991**, *30*, 330−332.
(15) Komuro, T.; Kawaguchi, H.; Tatsumi, K. *Inorg. Chem.* **2002**, *41*, 5083−5090.

Table 2. Selected Interatomic Distances (Å) and Angles (deg) for [(^{t}Bu$_3$SiS)Fe]$_2$(μ-SSi^{t}Bu$_3$)$_2$ (**1**$_2$), (^{t}Bu$_3$SiS)$_2$Fe(THF)$_2$ (**1**−(THF)$_2$), [Br$_2$Fe](μ-SSi^{t}Bu$_3$)$_2$[FeBr(THF)]Na(THF)$_4$ (**3**−Br), and *cis*-[(THF)IFe]$_2$(μ-SSi^{t}Bu$_3$)$_2$ (**4**)

	1$_2$	**1**−(THF)$_2$	**3**−Br	**4**
Fe···Fe	2.982(2)		3.460(4)	3.374(3)
Fe−S$_b$	2.323(2)		2.382(3),[a,b]	2.358(3),[a,b]
			2.387(3)[a,c]	2.356(3)[a,c]
	2.333(2)		2.348(3),[b,d]	2.374(3),[b,d]
			2.347(3)[c,d]	2.351(3)[c,d]
Fe−S$_t$	2.218(2)	2.271(2)		
		2.289(2)		
Fe−X			2.403(2),[a,e]	2.5717(12)
			2.408(2)[a,f]	
			2.379(2)[d]	2.5933(13)
Fe−O		2.094(3)	2.026(7)[d]	2.062(6)[a]
		2.136(3)		2.011(5)[d]
Na−Br			3.011(4),[e]	
			3.232(4)[f]	
Na−O			2.35(4)$_{ave}$	
Fe−S−Fe	79.64(7)		93.9(1),[b]	90.96(10),[b]
			94.1(1)[c]	91.58(11)[c]
S$_b$-Fe−S$_b$	100.11(7)		85.2(1),[a]	87.24(8),[a]
			86.8(1)[d]	86.98(8)[d]
S$_t$-Fe−S$_t$		137.33(5)		
S$_b$-Fe−S$_t$	128.65(8)			
	129.62(8)			
S−Fe−X			113.7(2),[a,b,e]	122.34(10),[a,b]
			112.0(2)[a,b,f]	123.99(9)[a,c]
			113.8(2),[a,c,e]	121.58(9),[b,d]
			111.0(2)[a,c,f]	124.95(9)[c,d]
			125.9(2),[b,d]	
			123.0(2)[c,d]	
S−Fe−O		100.72(9)	104.8(2)[b,d]	105.5(2)[a,b]
		102.74(8)	104.3(2)[c,d]	105.6(2)[a,c]
		104.53(8)		108.2(2)[b,d]
		113.00(9)		107.9(2)[c,d]
X−Fe−X			116.99(7)	
O−Fe−O		86.83(12)		
X−Fe−O			108.5(2)	109.2(2),[a]
				105.6(2)[d]
Fe−S$_t$−Si	115.79(9)	121.07(8)		
		125.33(6)		
Fe−S$_b$−Si	123.80(10)		133.9(2),[a,b]	132.6(2),[a,b]
			134.3(2)[a,c]	132.0(2)[a,c]
	127.37(10°)		131.2(2),[c,d]	133.3(2),[b,d]
			131.3(2)[b,d]	133.4(2)[c,d]
Fe−Br−Na			158.26(10),[e]	
			170.83(10)[f]	
Br−Na−Br			174.5(2)[e,f]	
O−Na−O			90.0(43)$_{ave}$	
			172.6(4),	
			179.8(4)	
O−Na−Br			90.0(46)$_{ave}$	

[a] Fe(1) distances. [b] Distances and angles to S(1). [c] Distances and angles to S(2). [d] Fe(2) distances. [e] Distances and angles to Br(3). [f] Distances and angles to Br(5).

yellow crystals of [Br$_2$Fe](μ-SSi^{t}Bu$_3$)$_2$[FeBr(THF)]Na(THF)$_4$ (**3**−Br, 86%) upon slow evaporation (eq 12). Degradation of a fresh sample of **3**−Br with a solution of DCl/D$_2$O in

$$2FeX_2(THF)_2 + 2{}^tBu_3SiSNa(THF)_x \xrightarrow[18-24\ h,\ 23\ °C]{THF,\ -NaX} [X_2Fe](\mu\text{-}SSi{}^tBu_3)_2[FeX(THF)]Na(THF)_4 \quad (12)$$

3−X, X = Cl, Br

D$_3$COD revealed a thiolate/THF ratio of 1:3.9, as determined by ^{1}H NMR spectroscopy. Visible desolvation of the crystals was noted when they remained at 23 °C for a few hours or when exposed to vacuum. Interpretation of the elemental analysis in view of the evident desolvation was problematic, and ^{1}H NMR spectra in THF-d_8 revealed only a single broad feature at δ 12.46 ($\nu_{1/2} \approx 280$ Hz); hence, the formula shown was obtained from the X-ray crystallographic study below. With this structure in hand, the elemental analysis may be interpreted as corresponding to a partially desolvated **3**−Br (i.e., [Br$_2$Fe](μ-SSi^{t}Bu$_3$)$_2$[FeBr(THF)]Na(THF)). Since the compound is a polymer in the solid state, it is likely that the spectra correspond to the [Br$_2$Fe](μ-SSi^{t}Bu$_3$)$_2$[FeBr(THF)]$^-$ anion. Evans' method[16] investigations were consistent with high-spin Fe(II) centers, as a μ_{eff}/Fe of 4.5 μ_B was determined.

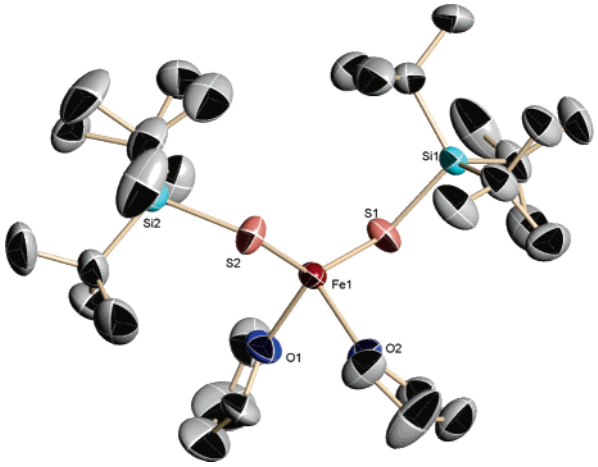

Figure 2. Molecular view of (^{t}Bu$_3$SiS)$_2$Fe(THF)$_2$ (**1**−(THF)$_2$).

A mixture of FeCl$_2$(THF)$_2$ and 1 equiv of ^{t}Bu$_3$SiSNa(THF)$_x$ produced yellow crystals of [Cl$_2$Fe](μ-SSi^{t}Bu$_3$)$_2$[FeCl(THF)]Na(THF)$_4$ (**3**−Cl, 74%), which was assigned its formula on the basis of characteristics related to **3**−Br. Degradation of **3**−Cl with DCl/D$_2$O in D$_3$COD provided the same 1:3.9 thiolate/THF ratio, and desolvation was also noted. Elemental analysis on one particular sample was consistent with a desolvated version, i.e., [Cl$_2$Fe](μ-SSi^{t}Bu$_3$)$_2$[FeCl(THF)]Na. ^{1}H NMR spectroscopy in THF-d_8 revealed a broad resonance at δ 9.11 ($\nu_{1/2} \approx 940$ Hz), and Evans' method[16] studies gave a μ_{eff}/Fe of 4.8 μ_B, again consistent with high-spin ferrous centers.

3.2. Structure of [Br$_2$Fe](μ-SSi^{t}Bu$_3$)$_2$[FeBr(THF)]Na(THF)$_4$ (3−Br). Crystal and refinement data are given in Table 1, and pertinent interatomic distances and angles are provided in Table 2. Although the data for **3**−Br is marginal, perhaps due to twinning problems inferred from broad reflections, the critical metric parameters are reasonable despite a severe disorder of the ^{t}Bu groups. Somewhat surprisingly, as Figure 3 indicates, **3**−Br possesses a polymeric structure in the solid state, as the square planar Na(THF)$_4$ unit is complexed by axial μ-Br ligands derived from the FeBr$_2$ side of the anion to form a zigzag chain. Bond distances and angles of the pseudo-tetrahedral Fe(II) centers were normal, and the iron−iron distance of 3.460(4) Å precludes significant through-space interaction.[17]

(16) (a) Evans, D. F. *J. Chem. Soc.* **1959**, 2003−2005. (b) Sur, S. K. *J. Magn. Reson.* **1989**, *82*, 169−173. (c) Schubert, E. M. *J. Chem. Educ.* **1992**, *69*, 62.

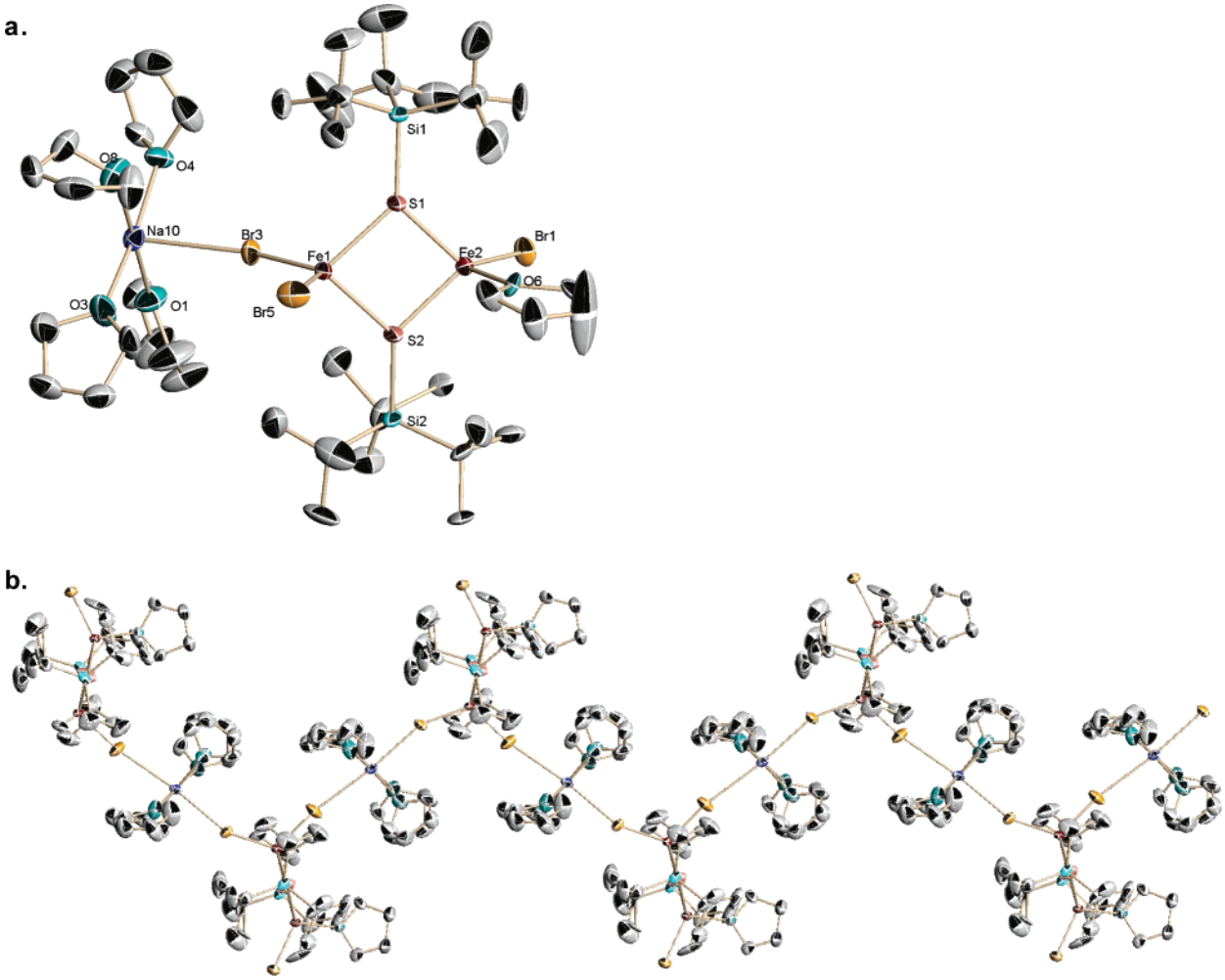

Figure 3. Molecular views of $[Br_2Fe](\mu\text{-}SSi^tBu_3)_2[FeBr(THF)]Na(THF)_4$ (**3**−Br): (a) a "monomer" unit, consisting of a $[Br_2Fe](\mu\text{-}SSi^tBu_3)_2[FeBr(THF)]^-$ anion paired with a $Na(THF)_4$ cation, and (b) the zigzag chain showing cations bound to the $FeBr_2$ end of the anion.

The *d*(Fe−μ-S) distances are slightly longer (2.382(3), 2.387(3) Å vs 2.348(3), 2.347(3) Å) to the iron (Fe1) containing the Na-associated bromides, whose Fe1−(μ-Br) distances (2.403(2), 2.408(2) Å) are slightly longer than the Fe2−Br bond length of 2.379(2) Å. Presumably, this is a consequence of greater anionic character in the $Br_2Fe(1)$-(μ-SR)$_2$ side. The iron−oxygen distance is 2.026(7) Å, which is significantly shorter than that in **1**−$(THF)_2$. The ligation of the bromides to Na^+ is nearly linear (i.e., Br−Na−Br = 174.5(2)°), while asymmetric Na−Br interactions are noted (Br3, 3.011(4); Br5, 3.232(4) Å), and the chain is somewhat kinked from iron to iron (Fe1−Br3−Na = 158.26(10)°, Fe1−Br5−Na = 170.83(10)°). The diamond core is slightly splayed at sulfur (Fe−S−Fe = 93.9(1)°, 94.1(1)°; S−Fe−S = 85.2(1)°, 86.8(1)°), and the polymer end of the dinuclear anion has large Br3−Fe1−Br5 (117.0(1)°) and S−Fe1−Br (112.6(14)°$_{ave}$) angles. The remaining side of the core manifests opened S−Fe2−Br angles (124.5(21)°$_{ave}$) and smaller ones involving the THF oxygen: O6−Fe2−S1/S2 = 104.8(2)°, 104.3(2)° and Br1−Fe2−O6 = 108.5(2)°.

3.3. *cis*-[(THF)IFe]$_2$(μ-SSi^{t}Bu$_3$)$_2$ (4). Unlike the chloride and bromide, when $FeI_2(THF)_2$ was treated with 1 equiv of $^tBu_3SiSNa(THF)_x$ in THF, no white material precipitated from the yellow solution. Solvent removal, thermolysis, and crystallization from benzene afforded yellow crystalline **4** in 75% yield (eq 13). It seems plausible that a dianionic dimer such as

$$2FeI_2(THF)_2 + 2{}^tBu_3SiSNa(THF)_x \xrightarrow[24\ h,\ 23\ °C]{1)\ THF} \xrightarrow[3)\ C_6H_6]{2)\ -THF,\ \Delta} \underset{\mathbf{4}}{cis\text{-}[(THF)IFe]_2(\mu\text{-}SSi^tBu_3)_2} \quad (13)$$

$[\{I_2Fe\}_2(\mu\text{-}SSi^tBu_3)_2][Na(THF)_x]_2$ formed initially, and only upon removal of solvent did loss of NaI occur. Dimer **4** did not exhibit significant desolvation and DCl/D_2O degradation in CD_3OD led to a thiolate/THF ratio of 1:1 by ^1H NMR analysis. The magnetic moment at room temperature was 4.8 μ_B/Fe as expected for two noninteracting ferrous centers.[16]

3.4. Structure of *cis*-[(THF)IFe]$_2$(μ-SSi^{t}Bu$_3$)$_2$ (4). Table 1 contains crystal and data collection information for **4**, while Table 2 provides some interatomic distances and angles. As Figure 4 illustrates, **4** has the expected edge-shared ditetrahedral geometry with bridging thiolates but possesses C_{2v} symmetry. Non-centrosymmetric dimers without chelating groups are unusual, but it is unclear why. Since both plausible geometries (i.e., cis, C_{2v} and trans C_{2h}) possess the same

(17) Cotton, F. A.; Walton, R. A. *Multiple Bonds Between Metal Atoms.* Oxford University Press: New York, 1993.

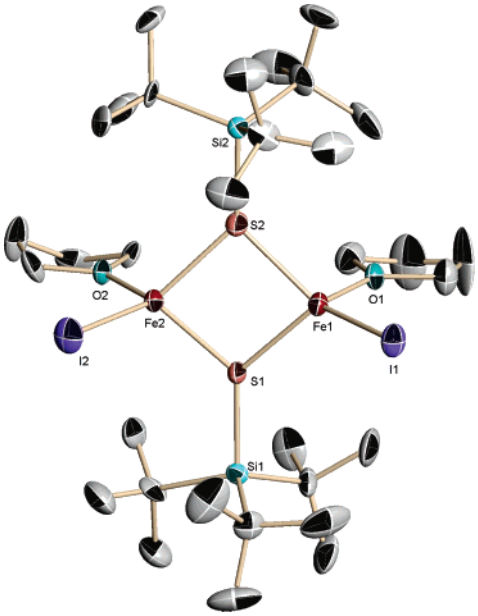

Figure 4. Molecular view of *cis*-[(THF)IFe]$_2$(μ-SSi^{t}Bu$_3$)$_2$ (**4**).

rotational symmetry,[18] they must be entropically similar, and there is no obvious enthalpy advantage for either. Perhaps intermolecular dipole−dipole interactions provide a favorable situation, since **4** crystallizes in the centrosymmetric orthorhombic space group *Pna*2$_1$.

The Fe−Fe interatomic distance is 3.374(3) Å, which precludes any significant Fe−Fe interaction,[17] and the bond lengths and angles in the dimer are normal. The *d*(FeI) are 2.5933(13) and 2.5717(12) Å, the iron−sulfur distances average 2.360(3) Å, and the *d*(Fe−O) are 2.062(6) and 2.011(5) Å, all values consistent with a ferrous iron. As the S−Fe−S (86.98(8)° and 87.24(8)°) and Fe−S−Fe (90.96(10)° and 91.58(11)°) angles show, the Fe$_2$(μ-S)$_2$ diamond core is slightly puckered in response to steric interactions between THF and the ^{t}Bu$_3$SiS groups. The O−Fe−I angles are 109.19(15)° and 105.57(15)°, while the I−Fe−S angles (123.2(15)°$_{ave}$) are splayed to a far greater extent than the O−Fe−S angles (106.8(14)°$_{ave}$).

4. Cyclic Oligomer Synthesis. 4.1. [Fe(μ-X)(μ-SSi^{t}Bu$_3$)]$_{12}$-(C$_6$H$_6$)$_n$ (5−FeX, X = Cl, Br). Solid **3**−Br was heated at 79°C under vacuum for 2 h and extracted with benzene to produce yellow crystals of **5**−FeBr in 72% yield (eq 14) after filtration. Degradation of the crystals with a solution of DCl/D$_2$O in D$_3$COD revealed a thiolate/THF/C$_6$H$_6$ ratio of 1.0:0.0:1.0, as determined by ^{1}H NMR spectroscopic integration. Complete

$$\underset{\mathbf{3}-\mathrm{X},\ \mathrm{X}=\mathrm{Cl,\ Br}}{[\mathrm{X_2Fe}](\mu\text{-}\mathrm{SSi}^t\mathrm{Bu_3})_2[\mathrm{FeX(THF)}]\mathrm{Na(THF)_4}} \xrightarrow[2)\ \text{benzene}]{1)\ 80°\mathrm{C,\ vacuum,\ 1.5-2\ h,\ -THF,\ -NaX}} \underset{\mathbf{5}-\mathrm{FeX},\ \mathrm{X}=\mathrm{Cl,\ Br}}{[\mathrm{Fe}(\mu\text{-}\mathrm{X})(\mu\text{-}\mathrm{SSi}^t\mathrm{Bu_3})]_{12}(\mathrm{C_6H_6})_n} \quad (14)$$

THF desolvation had occurred. The remaining material proved to be only partially soluble in C$_6$D$_6$, and a broad resonance was observable at δ 4.84 ($\upsilon_{1/2} \approx 60$ Hz). It is uncertain whether this signal corresponds to **5**−FeBr or a small impurity or decomposition product. Elemental analysis was consistent with the empirical formula [FeBr(SSi^{t}Bu$_3$)], but the low solubility precluded molecular weight studies; hence, a single-crystal X-ray structure determination proved necessary.

Thermal desolvation of solid **3**−Cl at 80 °C under vacuum for 1.5 h followed by benzene extraction and filtration gave yellow crystalline **5**−FeCl in moderate yield (42%, eq 14). Degradation by DCl/D$_2$O in CD$_3$OD permitted ^{1}H NMR analysis of the thiolate/THF/C$_6$H$_6$ ratio to be 1.0:0.0:0.6, which again indicated complete removal of THF. Elemental analysis was roughly consistent with the empirical formula [FeCl(SSi^{t}Bu$_3$)], but for **5**−FeCl, no resonance was observable in C$_6$D$_6$ solution due to insolubility. Since its solubility appeared distinct from **5**−FeBr and the thiolate/benzene degradation ratio was different, a single-crystal X-ray structure determination was conducted on **5**−FeCl.

4.2. [Fe(μ-I)(μ-SSi^{t}Bu$_3$)]$_{14}$(C$_6$H$_6$)$_n$ (6−FeI). Solid **4** was heated at 117 °C under vacuum for 5 h and extracted into benzene. Dark yellow crystals of **6**−FeI were isolated in poor yield (16%) upon slow evaporation. The formulation is

$$\underset{\mathbf{4}}{\textit{cis}\text{-}[(\mathrm{THF})\mathrm{IFe}]_2(\mu\text{-}\mathrm{SSi}^t\mathrm{Bu_3})_2} \xrightarrow[2)\ \text{benzene}]{1)\ 117\ °\mathrm{C,\ vacuum,\ 5\ h,\ -THF}} \underset{\mathbf{6}-\mathrm{FeI}}{[\mathrm{Fe}(\mu\text{-}\mathrm{I})(\mu\text{-}\mathrm{SSi}^t\mathrm{Bu_3})]_{14}(\mathrm{C_6H_6})_n} \quad (15)$$

based on its degradation by DCl/D$_2$O in D$_3$COD, which established a thiolate/THF/benzene ratio of 1.0:0.0:0.9 ratio according to ^{1}H NMR spectral analysis. Elemental analysis failed despite submission of well-defined, large crystals.

4.3. [Co(μ-Cl)(μ-SSi^{t}Bu$_3$)]$_{12}$(C$_6$H$_6$)$_6$ (5−CoCl). Since a practical recipe for aggregation was discovered, the methods were extended to the remaining first row "group VIII" metals. A THF mixture of anhydrous CoCl$_2$ and ^{t}Bu$_3$SiSNa(THF)$_x$ was stirred for 12 h to provide a blue solution. The THF was removed and the resulting blue material, conceivably the Co version of **3**−Cl or **4**, turned emerald green upon thermolysis under vacuum. Benzene extraction and filtration afforded green crystals of

$$\mathrm{CoCl_2} + {}^t\mathrm{Bu_3SiSNa(THF)}_x \xrightarrow[3)\ \text{benzene}]{\begin{array}{c}1)\ \mathrm{THF,\ 23\ °C,\ 12\ h}\\ 2)\ 81°\mathrm{C,\ 1.5\ h\ vacuum,}\\ \mathrm{-THF,\ -NaX}\end{array}} \underset{\mathbf{5}-\mathrm{CoCl}}{[\mathrm{Co}(\mu\text{-}\mathrm{Cl})(\mu\text{-}\mathrm{SSi}^t\mathrm{Bu_3})]_{12}(\mathrm{C_6H_6})_6} \quad (16)$$

5−CoCl in modest yield (21%, eq 16). Degradation of **5**−CoCl by DCl/D$_2$O in D$_3$COD revealed a thiolate/THF/C$_6$H$_6$ ratio of 1.0:0.0:0.5. Elemental analysis was consistent with the empirical formula [CoCl(SSi^{t}Bu$_3$)], and its structure was determined by single-crystal X-ray diffraction methods.

4.4. [Ni(μ-Br)(μ-SSi^{t}Bu$_3$)]$_{12}$(solvent)$_n$ (5−NiBr). Synthesis of a related nickelous cyclic oligomer was not straightforward. The combination of NiBr$_2$(THF)$_2$ and ^{t}Bu$_3$SiSNa-(THF)$_x$ in THF produced a green solution, but thermal

(18) Lowry, T. H.; Richardson, K. S. *Mechanism and Theory in Organic Chemistry*, 3rd ed.; Harper and Row: New York, 1987.

Table 3. Crystallographic Data for [Fe(μ-Cl)(μ-SSi^{t}Bu$_3$)]$_{12}$(C$_6$H$_6$)$_7$ (**5**−FeCl), [Co(μ-Cl)(μ-SSi^{t}Bu$_3$)]$_{12}$(C$_6$H$_6$)$_6$ (**5**−CoCl), [Fe(μ-Br)(μ-SSi^{t}Bu$_3$)]$_{12}$ (**5**−FeBr), [Ni(μ-Br)(μ-SSi^{t}Bu$_3$)]$_{12}$ (**5**−NiBr), and [Fe(μ-I)(μ-SSi^{t}Bu$_3$)]$_{14}$ (**6**−FeI)[a]

	5−FeCl	**5**−CoCl	**5**−FeBr	**5**−NiBr	**6**−FeI
formula	$C_{46.5}H_{91.5}Si_3S_3Cl_3Fe_3$	$C_{45}H_{90}Si_3S_3Cl_3Co_3$	$C_{36}H_{81}Si_3S_3Fe_3Br_3$	$C_{24}H_{54}Si_2S_2Ni_2Br_2$	$C_{50}H_{99.5}Si_{3.5}S_{3.5}Fe_{3.5}I_{3.5}$
fw	1105.08	1094.79	1101.74	740.24	1550.99
space group	$P\bar{4}2_1c$	$P\bar{4}2_1c$	$P\bar{4}2_1c$	$P6_3mc$	$Cmca$
Z	8	8	8	12	16
a, Å	23.3716(7)	23.287(3)	24.542(5)	26.128(16)	38.173(6)
b, Å	23.3716(7)	23.287(3)	24.542(5)	26.128(16)	24.296(4)
c, Å	24.0912(11)	24.155(4)	24.086(8)	24.69(2)	35.977(5)
α, deg	90	90	90	90	90
β, deg	90	90	90	90	90
γ, deg	90	90	90	120	90
V, Å^3	13159.4(8)	13098(3)	13349(6)	14597(18)	33367(9)
ρ_{calc}, g·cm^{-3}	1.116	1.110	1.096	1.010	1.235
μ, mm^{-1}	0.950	1.048	2.605	2.559	2.055
temp, K	173(2)	173(2)	173(2)	173(2)	173(2)
λ (Å)	0.71073	0.71073	0.71073	0.71073	0.71073
R ind	R1 = 0.0432	R1 = 0.0533	R1 = 0.0615	R1 = 0.1491	R1 = 0.0762
$[I > 2\sigma(I)]$[b,c]	wR2 = 0.1080	wR2 = 0.1255	wR2 = 0.1414	wR2 = 0.3646	wR2 = 0.1952
R ind	R1 = 0.0612	R1 = 0.0717	R1 = 0.0895	R1 = 0.2261	R1 = 0.1272
(all data)[b,c]	wR2 = 0.1116	wR2 = 0.1338	wR2 = 0.1592	wR2 = 0.4001	wR2 = 0.2390
GOF[d]	1.075	1.013	0.793	1.128	1.067

[a] For explanations regarding the variable amounts of benzene of solvation, see the text and Experimental Section. [b] $R1 = \sum||F_o| - |F_c||/\sum|F_o|$. [c] $wR2 = [\sum w(|F_o| - |F_c|)^2/\sum wF_o^2]^{1/2}$. [d] GOF (all data) $= [\sum w(|F_o| - |F_c|)^2/(n - p)]^{1/2}$, n = number of independent reflections, p = number of parameters.

desolvation and benzene extraction of the resulting green solid led to a complex mixture in which red **5**−NiBr and purple [(^{t}Bu$_3$SiS)Ni]$_2$(μ-SSi^{t}Bu$_3$)$_2$ (**7**, eq17)

$$\mathrm{NiBr_2(THF)_2} + {}^t\mathrm{Bu_3SiSNa(THF)}_x \xrightarrow[\text{3) benzene or hexane}]{\text{1) THF, 23°C, 16 h; 2) 88 °C, 3 h vacuum, −THF, −NaX}} [\mathrm{Ni}(\mu\text{-Br})(\mu\text{-SSi}^t\mathrm{Bu_3})]_{12}(\mathrm{C_6H_6})_n\ (\mathbf{5}\text{−NiBr}) + [({}^t\mathrm{Bu_3SiS})\mathrm{Ni}]_2(\mu\text{-SSi}^t\mathrm{Bu_3})_2\ (\mathbf{7}) + \cdots \quad (17)$$

$$\mathrm{NiBr_2(THF)_2} + 2\,{}^t\mathrm{Bu_3SiSNa(THF)}_x \xrightarrow[\text{24 h, − 2NaBr}]{\text{THF}} \underset{\mathbf{7}}{[({}^t\mathrm{Bu_3SiS})\mathrm{Ni}]_2(\mu\text{-SSi}^t\mathrm{Bu_3})_2} \quad (18)$$

were ultimately identified. Diamagnetic, purple crystalline **7** was synthesized from $NiBr_2(THF)_2$ and 2 equiv of the thiolate in 63% yield (eq 18). ^{1}H and ^{13}C{^{1}H} NMR spectra of **7** revealed two ^{t}Bu$_3$Si moieties, and molecular weight studies by the Signer isopiestic method were indicative of a dimer.[13−15]

The reaction of $NiBr_2(THF)_2$ and 1 equiv of thiolate was assayed prior to desolvation by removing THF and crystallizing a green product, tentatively formulated as as [(THF)BrNi]$_2$(μ-SSi^{t}Bu$_3$)$_2$ (**8**, eq 19).

$$\mathrm{NiBr_2(THF)_2} + {}^t\mathrm{Bu_3SiSNa(THF)}_x \xrightarrow[\text{16 h, −NaBr}]{\text{THF, 23 °C}} \underset{\mathbf{8}}{{}^1/_2[(\mathrm{THF})\mathrm{BrNi}]_2(\mu\text{-SSi}^t\mathrm{Bu_3})_2} \quad (19)$$

Rapid desolvation prevented standard characterization of the compound, but a DCl/D$_2$O degradation in D$_3$COD afforded a 1.0:1.1 ratio of ^{t}Bu$_3$SiS/THF, hence the formulation. Dissolution of **8** in benzene-d_6 generated a purple solution of **7**, and a white precipitate, probably $NiBr_2$, was noted. Ligand disproportionation was occurring, and once noted in polar solvents, it was observed in the formation of **5**−NiBr as well. Thermolysis of the green solid in eq 19 led to a red-purple solid, but the purple dimer (**7**) could be washed away in Et$_2$O, and extraction in hexane led to a red solution from which **5**−NiBr crystallized in ∼15% yield. It was typically contaminated with small amounts of **7** and a white solid,

$$\underset{\mathbf{5}\text{−NiBr}}{[\mathrm{Ni}(\mu\text{-Br})(\mu\text{-SSi}^t\mathrm{Bu_3})]_{12}} \xrightarrow[\text{12 h}]{\text{hexane}} \mathrm{NiBr_2(s)} + \underset{\mathbf{7}}{[({}^t\mathrm{Bu_3SiS})\mathrm{Ni}]_2(\mu\text{-SSi}^t\mathrm{Bu_3})_2} \quad (20)$$

presumably $NiBr_2$, thereby precluding elemental analysis and bulk magnetic studies. If the red solution was allowed to stand overnight, it turned purple, indicative of the presence of **7** (eq 20), apparently formed via disproportionation.

5. Cyclic Oligomer Structures. X-ray structure determinations of the cyclic oligomers [M(μ-X)(μ-SSi^{t}Bu$_3$)]$_n$ (M = Fe, n = 12, X = Cl (**5**−FeCl), Br (**5**−FeBr); M = Fe, n = 14, X = I (**6**−FeI);[6] M = Co, n = 12, X = Cl (**5**−CoCl); M = Ni, n = 12, X = Br (**5**−NiBr))[7] have been previously communicated, but some comparison of the compounds is warranted. Table 3 provides an abbreviated list of the crystallographic data for the 12-membered wheels (**5**−MX) and the 14-membered ellipse (**6**−FeI), while Table 4 provides salient interatomic distances and angles. Note that there is a discrepancy between the number of solvent molecules implicated by the degradation studies in the previous section and those inferred by the formulas in Table 3, which are obtained from analysis of the diffraction data. The formulas and quality of the structures reflects the data quality and the disorder evident in the ^{t}Bu$_3$Si groups and solvent molecules. The quality is roughly **5**−FeCl ≥ **5**−CoCl > **5**−FeBr > **6**−FeI ≫ **5**−NiBr. The ferrous (**5**−FeCl) and cobaltous (**5**−CoCl) chloride wheels were well-ordered, and 2.5 benzenes of solvation in the asymmetric unit could be modeled with partial occupancies. Figure 5 illustrates pseudo-D_{6d} **5**−FeCl,

Table 4. Comparative Interatomic Distances (Å) and Angles (deg) for $[Fe(\mu\text{-}Cl)(\mu\text{-}SSi^tBu_3)]_{12}(C_6H_6)_7$ (**5**−FeCl), $[Co(\mu\text{-}Cl)(\mu\text{-}SSi^tBu_3)]_{12}(C_6H_6)_6$ (**5**−CoCl), $[Fe(\mu\text{-}Br)(\mu\text{-}SSi^tBu_3)]_{12}$ (**5**−FeBr), $[Ni(\mu\text{-}Br)(\mu\text{-}SSi^tBu_3)]_{12}$ (5-NiBr), and $[Fe(\mu\text{-}I)(\mu\text{-}SSi^tBu_3)]_{14}$ (**6**−FeI)

	5−FeCl	**5**−CoCl	**5**−FeBr	**5**−NiBr	**6**−FeI
$M\cdots M_{ave}$	3.127(44)	3.115(40)	3.171(51)	3.314(41)	3.238(46)[a]
X···X	9.484(29) (ave)	9.614(27) (ave)	9.483(22) (ave)	10.750(8)	13.469(2)
				9.583(8)	12.402(2)
					11.499(2)
					11.101(2)
$M-X_{ave}$	2.338(9)	2.310(11)	2.474(9)	2.440(9)	2.672(11)
$M-S_{ave}$	2.340(9)	2.305(9)	2.339(9)	2.276(53)	2.342(7)
$M-X-M_{ave}$	83.9(15)	84.8(13)	79.7(17)	85.5(15)	74.6(13)
$M-S-M_{ave}$	83.9(14)	85.0(12)	85.4(18)	93.9(11)	87.4(16)
$X-M-X_{ave}$	103.5(13)	107.8(13)	103.6(15)	103.3(1)	101.6(7)
$S-M-S_{ave}$	124.8(6)	126.6(15)	127.4(8)	137.0(26)	126.8(36)[b]
$X-M-S_{ave}$[c]	93.3(5)	91.9(4)	94.7(7)	88.8(17)	96.9(8)
$X-M-S_{ave}$[d]	121.0(14)	119.7(12)	117.7(13)	118.4(21)	116.2(17)[e]

[a] Individual *d*(Fe···Fe): 3.183(4), 3.217(4), 3.270(4), 3.280(4) Å. [b] The S(3)−Fe(4)−S(4) angle nearest the foci of the ellipse is 132.13(17)°, whereas the remaining S−Fe−S angles are 124.6(2)°, 126.05(16)°, and 124.49(16)°. [c] Endo X−M−S angles. [d] Exo X−M−S angles. [e] The S(3)−Fe(4)−I(4) and S(4)−Fe(4)−I(3) angles nearest the foci of the ellipse are 112.85(12)° and 115.35(16)°, respectively, whereas the remaining S−Fe−I angles average 117.1(7)°.

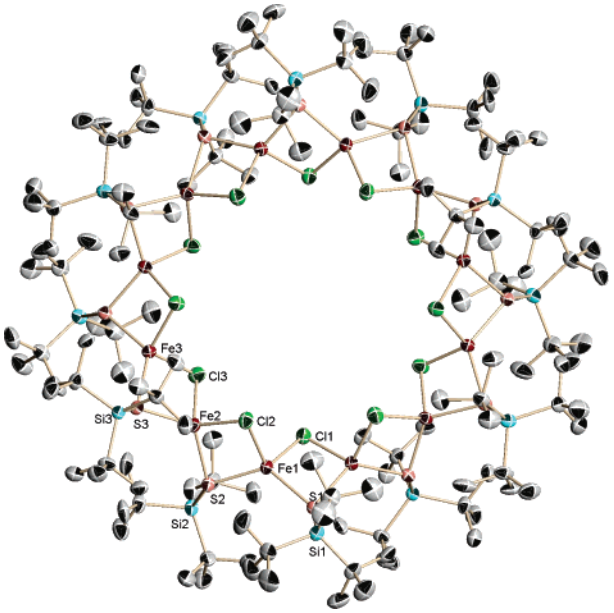

Figure 5. Molecular view of pseudo-D_{6d} $[Fe(\mu\text{-}Cl)(\mu\text{-}SSi^tBu_3)]_{12}(C_6H_6)_7$ (**5**−FeCl).

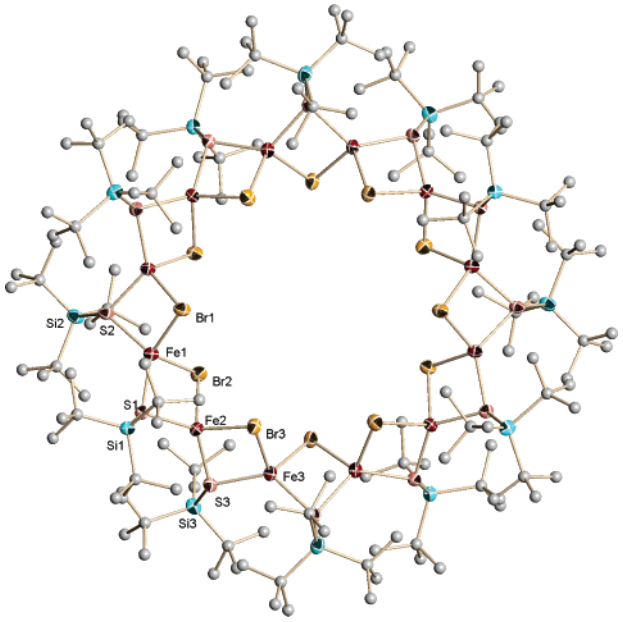

Figure 6. Molecular view of pseudo-D_{6d} $[Fe(\mu\text{-}Br)(\mu\text{-}SSi^tBu_3)]_{12}$ (**5**−FeBr).

whose metric parameters are very close to **5**−CoCl, which has been illustrated previously.[7] The peripheral carbons in the ^{t}Bu groups of pseudo-D_{6d} **5**−FeBr were refined isotropically, as Figure 6 shows, and yet no disorder model could be found, which is probably why the GOF is so poor. In addition, the unit cell had two cavities of disordered benzenes of solvation that could not be modeled; hence, refinement required the use of SQUEEZE,[19] and the final model only reflects the ordered part of the cell. The poor data quality of pseudo-C_{6v} **5**−NiBr (Figure 7) necessitated the use of geometric constraints in the ^{t}Bu$_3$SiS groups, and SQUEEZE was also needed, since the two cavities in the cell possessed large amounts of disordered solvent molecules that could not be modeled. The ellipse, **6**−FeI, possesses idealized C_{2h} symmetry, as Figure 8 reveals, and also required isotropic refinement of the ^{t}Bu groups and employment of SQUEEZE because disordered solvent molecules in the cell cavities could not be modeled. The final model reflects only the ordered part of the molecule devoid of solvent contribution.

Although **5**−FeCl, **5**−CoCl, and **5**−FeBr crystallize in a primitive tetragonal cell (the asymmetric unit is a quarter wheel), their arrangement within the cell is essentially body-centered, with two wheels per unit cell. Figure 9 shows the columnar stacking of the **5**−FeBr wheel, which includes a channel down the center of the wheels and a smaller one between stacks consisting of the alternating square arrays of wheels. Benzenes have been located in the large channel and feature edge-to-face stacking,[20,21] as previously shown.[7] The lattice parameters of **5**−FeCl and **5**−CoCl are virtually identical (within ∼0.5%), reflecting the similarity in radii between Fe (r_{cov}(Fe) = 1.17, r_{cov}(Co) = 1.16 Å) and Co. The switch from Cl to Br causes a very modest increase in

(19) Vandersluis, P.; Spek, A. L. *Acta Crystallogr.* **1990**, *A46*, 194−201.

(20) Mecozzi, S.; West, A. P.; Dougherty, D. A. *Proc. Natl. Acad. Sci. U.S.A.* **1996**, *93*, 10566−10571.

(21) (a) Klebe, G.; Diederich, F. *Philos. Trans. R. Soc. London A* **1993**, *345*, 37−48. (b) Bacon, G. E.; Curry, N. A.; Wilson, S. A. *Proc. R. Soc. London A* **1964**, *279*, 98−110.

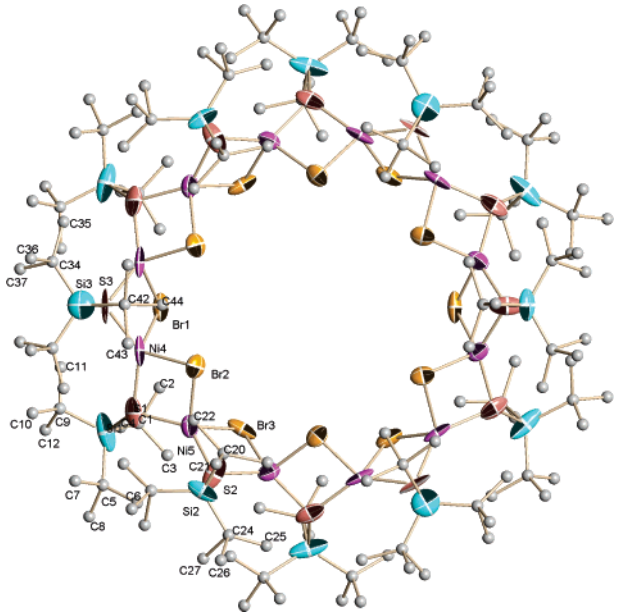

Figure 7. Molecular view of pseudo-C_{6v} [Ni(μ-Br)(μ-SSi^{t}Bu$_3$)]$_{12}$ (**5**−NiBr).

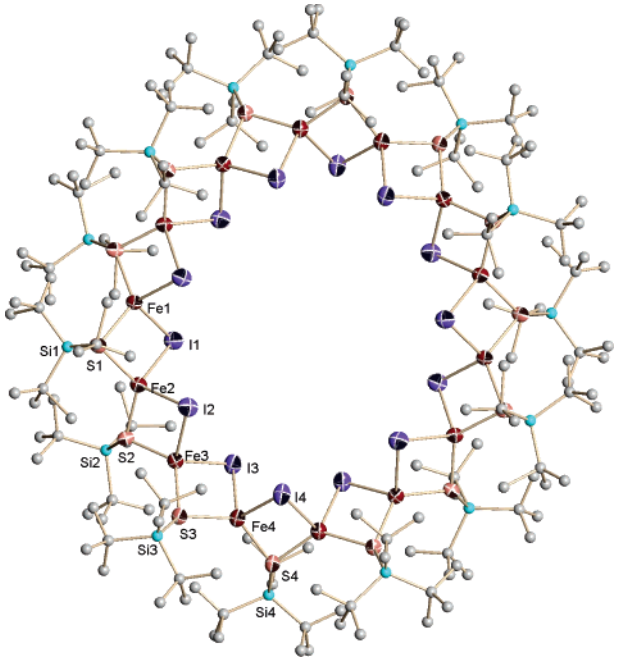

Figure 8. Molecular view of pseudo-C_{2h} [Fe(μ-I)(μ-SSi^{t}Bu$_3$)]$_{14}$ (**6**−FeI).

the wheel size, which is barely evident in the average Fe···Fe distance: **5**−FeBr, (3.171(51) Å) > **5**−FeCl (3.127(44) Å) > **5**−CoCl (3.115(40) Å). Curiously, while the $a = b$ unit cell parameters increase from **5**−CoCl (23.287(3) Å) to **5**−FeCl (23.3716(7) Å) to **5**−FeBr (24.542(5) Å) in line with the increasing sum of the covalent radii, the c parameter manifests the opposite trend. Although it is difficult to assay the role solvent plays in the unit cell parameters, it is perhaps the connectivity of the wheels that dictates this interplay. The wheels may be viewed as being composed of (S···X) edge-shared distorted tetrahedra, whose inner X_{12} "ring" features six halides above and below the M_{12} plane, hence the D_{6d} idealized symmetry. As the d(M−X) distances get shorter, the M···M distances get very slightly shorter and the "hinges" of the tetrahedral swing the ᵗBu$_3$SiS groups very slightly more "up and down" relative to the M_{12} plane, thereby increasing c at the expense of $a = b$.

The tetrahedra must "flex" in response to the d(M−X) because the transannular average d(X···X) of **5**−FeCl and **5**−FeBr are essentially identical despite major differences in covalent radii (r_{cov}(Cl) = 0.99, r_{cov}(Br) = 1.14 Å). The greater average d(Fe−Br) of 2.474(9) Å vs the average d(Fe−Cl) of 2.338(9) Å translates to a smaller average X−Fe−X angle and a larger average S−Fe−S angle for **5**−FeBr. The largest average X−M−X angles belong to **5**−CoCl, which has the shortest average d(M−X), as expected. In general, the wheels are remarkably similar, and the changes in distances and angles between them are quite subtle, as Table 3 reveals. Although the originally desired helical polymers of "ᵗBu$_3$SiSMX" have not formed, the "up and down" displacement of the ᵗBu$_3$SiS groups is essentially what was expected. What was not expected was the substantial degree to which the tetrahedral centers would angularly distort in order to form these cyclic oligomers while maintaining normal d(M−X) and d(M−S).

The nickel wheel, **5**−NiBr, is somewhat of an oddity because its secondary structure is subtly different than its congeners. As Figure 7 depicts, **5**−NiBr possesses idealized C_{6v} symmetry, with six alternating bromides pointing more toward the center of the wheel than the other six (d(Br···Br) = 9.583(8) vs 10.750(8) Å), which are more vertical with respect to the wheel plane. If there were questions regarding the templating of wheel formation with benzene, the formation of **5**−NiBr from hexane solution would appear to dismiss that view. The wheel is still 12-membered, but now the Ni center cannot accommodate the bigger halide with a small Br−Ni−Br angle (cf **5**−FeBr), whose average is 85.5(15)°, the largest of all the cyclic oligomers. The result is desymmetrization, a longer d(M···M) of 3.314(41) Å, and a change in packing that may derive from the "lopsided" wheel. There are still two molecules per unit cell, but **5**−NiBr crystallizes in a primitive hexagonal space group ($P6_3mc$) whose cell is roughly 10% larger than the tetragonal ones. The ABAB ordering of the hexagonal cell might be expected to pack more efficiently than the pseudo-body-centered arrangements of **5**−CoCl, **5**−FeCl, and **5**−FeBr, but the above factors—principally the larger wheel size and accompanying solvent packing—must counteract a standard packing argument. The hexagonal packing generates a different columnar array than the tetragonal cells. One small, smooth channel is comprised of the stacked trigonal holes that remain after ABAB packing, and another channel is composed of alternating wheel centers and trigonal holes. While templating wheel formation with benzene can be discounted on the basis of the existence of **5**−NiBr, the solvent change may be responsible for the shift from a pseudo-body-centered to hexagonal packed arrangement.

A diversion from the 12-membered rings occurs for M = Fe and X = I in the form of the ellipse, **6**−FeI shown in Figure 8. The accompanying change from tetragonal to

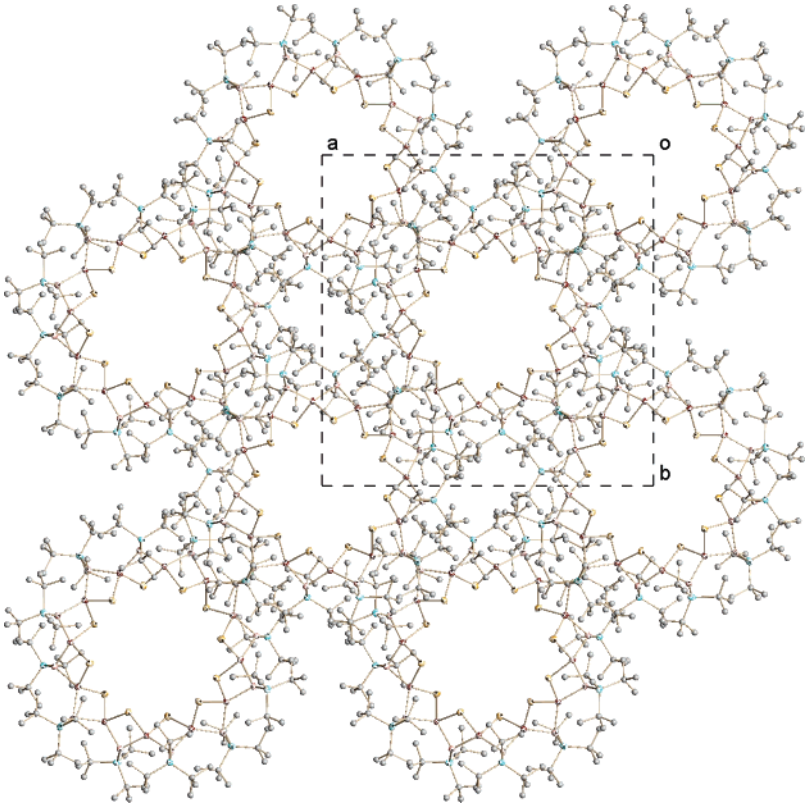

Figure 9. Columnar stacking of $[Fe(\mu\text{-Br})(\mu\text{-SSi}^t\text{Bu}_3)]_{12}$ (**5**−FeBr), with a dashed line for the top of the unit cell.

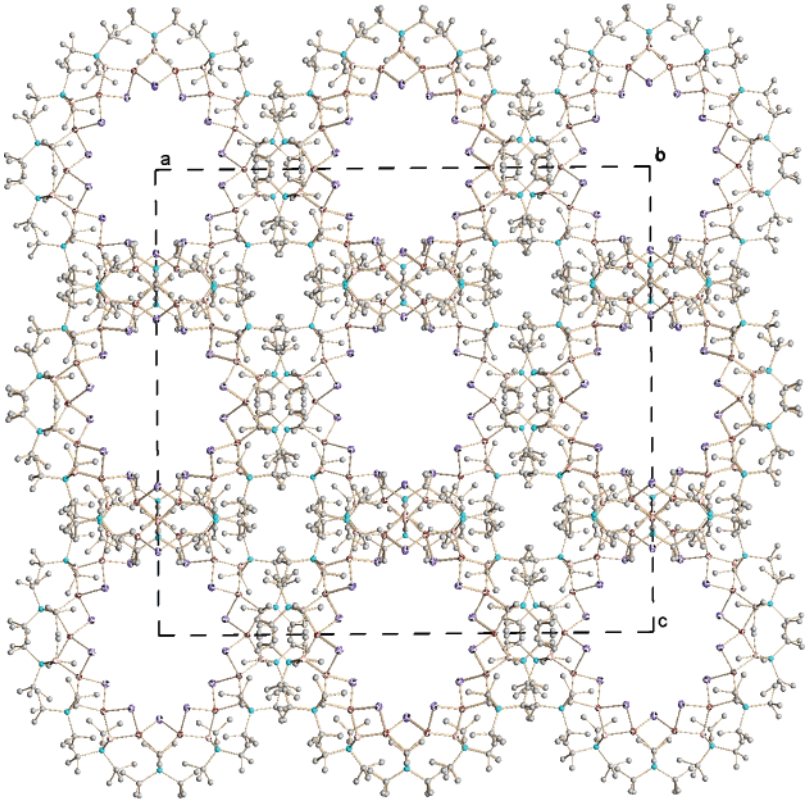

Figure 10. Columnar stacking of $[Fe(\mu\text{-I})(\mu\text{-SSi}^t\text{Bu}_3)]_{14}$ (**6**−FeI), with a dashed line for the top of the unit cell showing the *a* and *c* lengths.

orthorhombic cell doubles the number of molecules in the cell to four but leaves intact the pseudo-body-centered arrangement. Figure 10 illustrates the base-centered cell, but by rotating the top of the cell by roughly 45°, the packing can be seen as essentially the same as in **5**−FeCl, **5**−FeBr, and **5**−CoCl, and the same two types of channels—down and between the wheels—are evident. The ring has been opened up to accommodate the $d(\text{FeI})_{ave} = 2.672(11)$ Å that

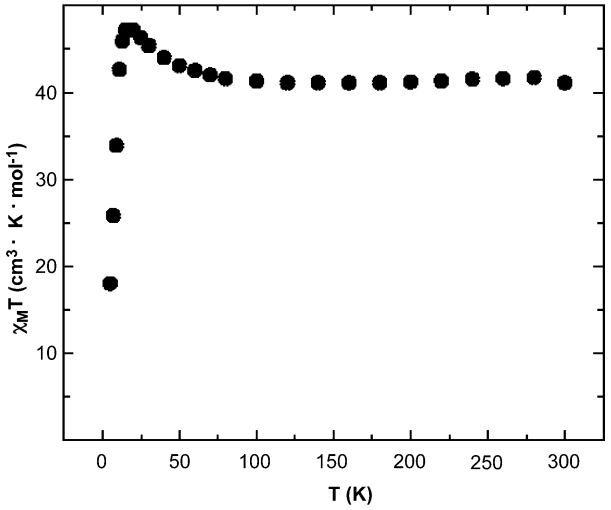

Figure 11. Plot of $\chi_M T$ vs T for [Fe(μ-Cl)(μ-SSi^{t}Bu$_3$)]$_{12}$ (**5**−FeCl) from 5 to 300K (1 T applied field).

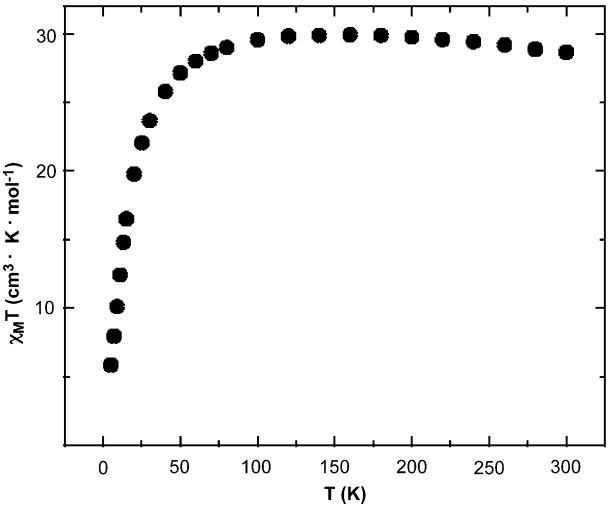

Figure 12. Plot of $\chi_M T$ vs T for [Fe(μ-Br)(μ-SSi^{t}Bu$_3$)]$_{12}$ (**5**−FeBr) from 5 to 300K (1 T applied field).

are substantially longer than $d(\mathrm{FeS})_{ave} = 2.342(7)$ Å, but the trans annular d(I···I) are still not much different: 11.101(2), 11.499(2), 12.402(2), and 13.469(2) Å. As Table 4 details, the tetrahedra nearest the foci exhibit effects due to additional strain, as the wheel kinks to adopt its secondary structure.

6. Magnetism of the Cyclic Oligomers. Variable-temperature magnetic susceptibility data were collected for microcrystalline samples of **5**−FeCl, **5**−FeBr, **5**−CoCl, and **6**−FeI. Fear of persistent contaminants in the nickelous bromide wheel (**5**−NiBr) obviated characterization of its magnetism. Plots of $\chi_M T$ vs T for the cyclic oligomers are depicted in Figures11−14. Upon decreasing the temperature of **5**−FeCl (Figure 11), the product $\chi_M T$ remains essentially unchanged at a value of 41 cm^3·K·mol^{-1} ($\mu_{eff} \approx 18\ \mu_B$) from 300 to 50 K, whereupon $\chi_M T$ slightly increases to a value of 47 cm^3·K·mol^{-1} ($\mu_{eff} \approx 19.5\ \mu_B$). Below 15 K, the value of $\chi_M T$ sharply decreases. The value of $\chi_M T$ for complex **5**−FeBr (Figure 12) also remains essentially unchanged from a value of 28 cm^3·K·mol^{-1} ($\mu_{eff} \approx 15.5\ \mu_B$) at 300 K down to 100 K, whereupon a smooth decrease of $\chi_M T$ is observed

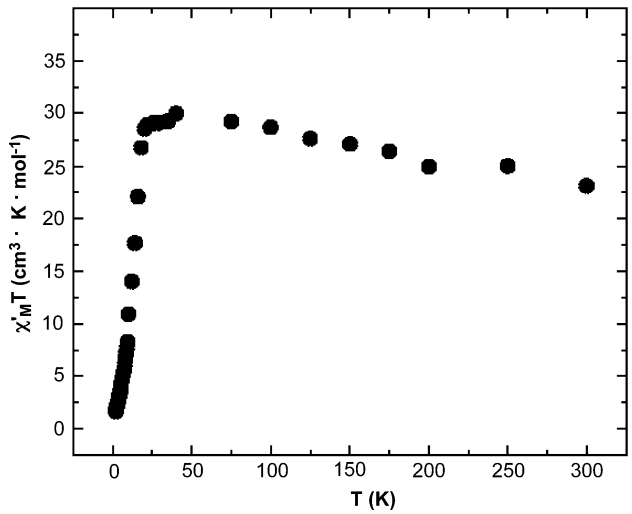

Figure 13. Plot of $\chi'_M T$ vs T for [Fe(μ-I)(μ-SSi^{t}Bu$_3$)]$_{14}$ (**6**−FeI) from 5 to 300K, where χ'_M is the molar in-phase *ac* susceptibility measured at 1000 Hz.

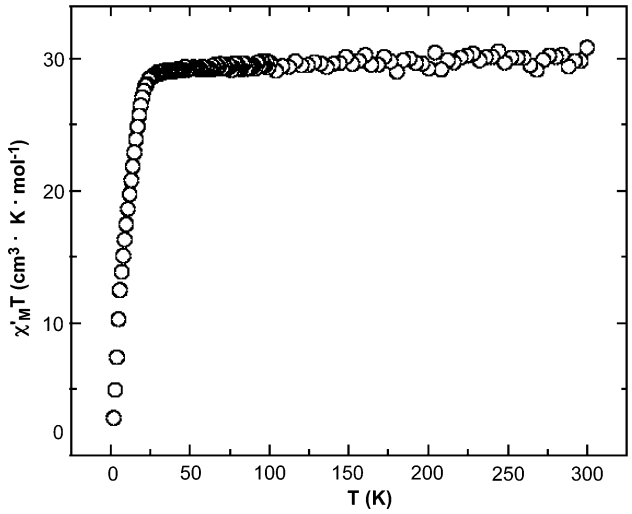

Figure 14. Plot of $\chi'_M T$ vs T for [Co(μ-Cl)(μ-SSi^{t}Bu$_3$)]$_{14}$ (**5**−CoCl) from 5 to 300K, where χ'_M is the molar in-phase *ac* susceptibility measured at 1000 Hz.

and continues until the lowest temperature of 5 K is reached. Complexes **6**−FeI and **5**−CoCl (Figures 13 and 14) exhibit a similar response in their $\chi'_M T$ vs T plots (χ'_M is the molar in-phase *ac* susceptibility). At 300 K, **6**−FeI and **5**−CoCl have $\chi'_M T$ values of 23 ($\mu_{eff} \approx 15\ \mu_B$) and 29 cm^3·K·mol^{-1} ($\mu_{eff} \approx 15.5\ \mu_B$), respectively. These values remain essentially unchanged with decreasing temperature until below 20 K where a sharp decrease is noted.

A quantitative analysis of the intermolecular magnetic exchange interactions between either the Fe(II) or Co(II) ions in these four complexes is not possible due to the fact that magnetic exchange interactions between pairs of Co(II) or Fe(II) ions are anisotropic. Tetrahedrally coordinated Fe(II) and Co(II) ions generally have large g-values where there is considerable g-tensor anisotropy. The presence of appreciable orbital angular momentum at these ions leads to anisotropic magnetic exchange interactions between metal centers. The simplifying models which describe the exchange as being in either the isotropic, Ising, or XY limits are inappropriate.

Detailed information on the single-ion anisotropy of each unique metal center involved in the magnetic exchange would be needed before any specific analysis of susceptibility data for these complexes could be attempted. The situation is further complicated by the existence of several unique Fe or Co ions in the asymmetric unit of each crystal structure. There are three unique Fe(II) or Co(II) atoms in complexes **5**−FeCl, **5**−FeBr, and **5**−CoCl, and **6**−FeI has four unique Fe(II) atoms, each requiring its own *g*- and *J*-tensor. In principle, one could extract single-ion anisotropy parameters by doping a diamagnetic host, i.e., a wheel composed of $[ZnCl]_{12}$, with a small amount of Fe(II) or Co(II), but such hosts have not been prepared despite considerable effort. Single-crystal high-frequency EPR and magnetometry experiments could then be performed, and a similar analysis has recently been performed on 1-D Co(II) polymers.[22]

Attempts to fit χ_M vs T plots with the Heisenberg infinite chain model[23] yielded consistent results, despite the intrinsic simplicity of the model. Reasonable fits of **5**−FeBr and **5**−CoCl were generated, and these wheels were weakly antiferromagnetic.[6] In modest contrast, the fit of **5**−FeCl was closest to that of a simple paramagnet. Although the Heisenberg chain model is strictly inappropriate, the interactions between crystallographically distinct metal centers in **5**−FeBr, **5**−CoCl, and **5**−FeBr must be very similar in order for it to have provided a reasonable approximation of each wheel's magnetism. Note that certain Fe(II) centers in **6**−FeI are significantly different, and here the chain model gave no reasonable fit.

Despite quantitative difficulties, one can make the qualitative observation that magnetic exchange interactions over the temperature range examined appear to be weak since there are only small variations of the product $\chi_M T$ until low temperatures. With the exception of **5**−FeCl, all interactions appear to be very weakly antiferromagnetic. Below 15 K, there is a precipitous drop of $\chi_M T$ toward zero. It is likely that this drop in the $\chi_M T$ value at low temperatures is due to zero-field splitting effects since tetrahedral Fe(II) and Co(II) ions generally exhibit appreciable single-ion zero-field interactions. It is intreresting that **5**−FeCl shows a weak ferromagnetic interaction between Fe(II) ions since it was anticipated that the insulating properties of the ligands would minimize intermolecular magnetic exchange interactions. It may be possible that spin canting is the source of this weak ferromagnetic interaction.[24] This phenomenon has been observed in a number of one-dimensional transition metal polymers.[25]

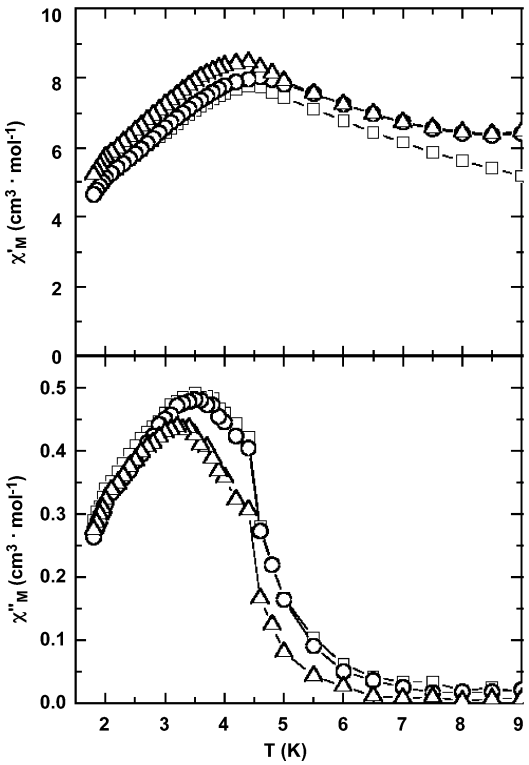

Figure 15. Plot of the molar in-phase (χ'_M) and molar out-of-phase (χ''_M) components for the *ac* susceptibility vs T for $[Fe(\mu\text{-Cl})(\mu\text{-SSi}^t\text{Bu}_3)]_{12}$ (**5**−FeCl). The measurement was performed with a 1 G field oscillating at the frequencies 1000 (squares), 500 (circles), and 50 Hz (triangles). The solid lines are meant to quide the eyes and do not represent a theoretical fit.

Out-of-phase *ac*-susceptibility data were collected for all four complexes, and the results are depicted in Figures15−17. The iron chloride (**5**−FeCl) and iodide (**6**−FeI) complexes both show out-of-phase *ac* responses beginning at ca. 5 K that are not frequency dependent. The values of χ''_M are essentially superimposable upon one another, despite the different frequencies probed (1000, 500, and 50 Hz). The cobalt chloride species (**5**−CoCl) exhibits a similar response; however, the temperature at which the χ''_M signal first appeared is ca. 20 K. The iron bromide wheel (**5**−FeBr) did not exhibit an out-of-phase component (not shown). The appearance of an out-of-phase peak in a plot of χ''_M vs T is often associated with single-molecule magnetism,[26,27] but it is not likely that this is the case here. The onset of the non-frequency-dependent χ''_M peak is accompanied by a cusp in the corresponding χ'_M vs T plots. Both observations suggest that there is likely a phase change at the temperatures where the out-of-phase feature is observed. Specific heat measurements would need to be performed to verify and ascertain the nature of this phase change.

Discussion

1. Synthetic Investigations. 1.1. ^{t}Bu$_3$SiSH. Two independent syntheses of ^{t}Bu$_3$SiSH and ^{t}Bu$_3$SiSNa have been

(22) (a) Caneschi, A.; Gatteschi, D.; Lalioti, N.; Sangregorio, C.; Sessoli, R.; Venturi, G.; Vindigni, A.; Rettori, A.; Pini, M. G.; Novak, M. A. *Angew. Chem., Int. Ed.* **2001**, *40*, 1760−1762. (b) Caneschi, A.; Gatteschi, D.; Lalioti, N.; Sorace, L.; Tangoulis, V.; Vindigni, A. *Chem. Eur. J.* **2002**, *8*, 286−292.

(23) (a) Smith, T.; Friedberg, S. A. *Phys. Rev.* **1968**, *176*, 660−665. (b) Dingle, R.; Lines, M. E.; Holt, S. L. *Phys. Rev.* **1969**, *187*, 643−648. (c) Wagner, G. R.; Friedberg, S. A. *Phys. Lett.* **1964**, *9*, 11−13.

(24) Carlin, R. L. *Magnetochemistry*; Springer-Verlag: Berlin; New York, 1986.

(25) (a) Herweijer, A.; de Jonge, W. J. M.; Botterman, A. C.; Bongaarts, A. L. M.; Cowen, J. A. *Phys. Rev. B.* **1972**, *B5*, 4618. (b) Kopinga, K.; van Vlimmeren, Q. A. G.; Bongaarts, A. L. M.; de Jonge W. J. M. *Physica* **1977**, *B86*−*88*, 671.

(26) *Molecular Magnetism*; Kahn, O., Ed.; VCH: New York, 1993.

(27) (a) Christou, G.; Gatteschi, D.; Hendrickson, D. N.; Sessoli, R. *MRS Bull.* **2000**, *25*, 66−71. (b) Gatteschi, D.; Sessoli, R. *J. Magn. Magn. Mater.* **2004**, *272*, 1030−1036. (c) Gatteschi, D.; Caneschi, A.; Pardi, L.; Sessoli, R. *Science* **1994**, *265*, 1054−1058.

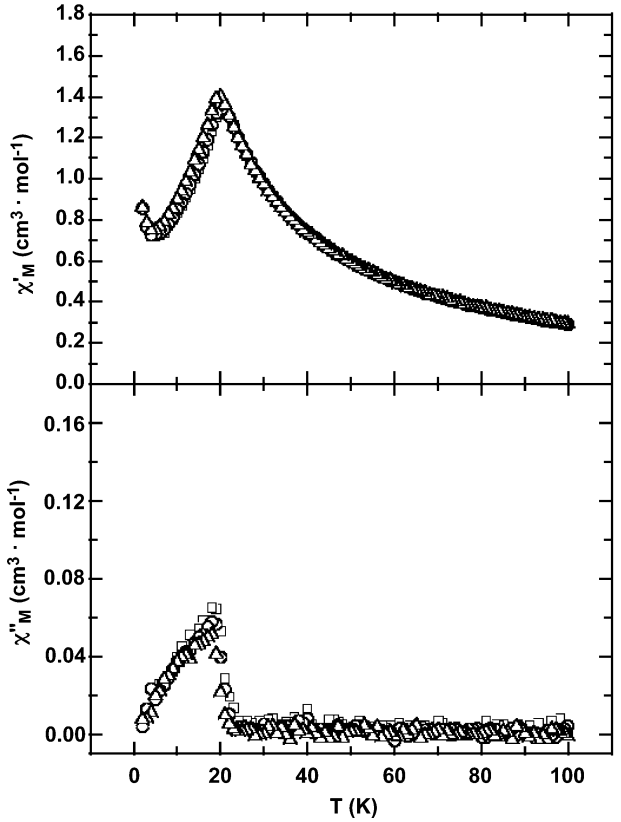

Figure 16. Plot of the molar in-phase (χ'_M) and molar out-of-phase (χ''_M) components for the *ac* susceptibility vs *T* for [Fe(μ-I)(μ-SSi^{t}Bu$_3$)]$_{14}$ (**6**−FeI). The measurement was performed with a 1 G field oscillating at the frequencies 1000 (squares), 500 (circles), and 50 Hz (triangles). The solid lines are meant to quide the eyes and do not represent a theoretical fit.

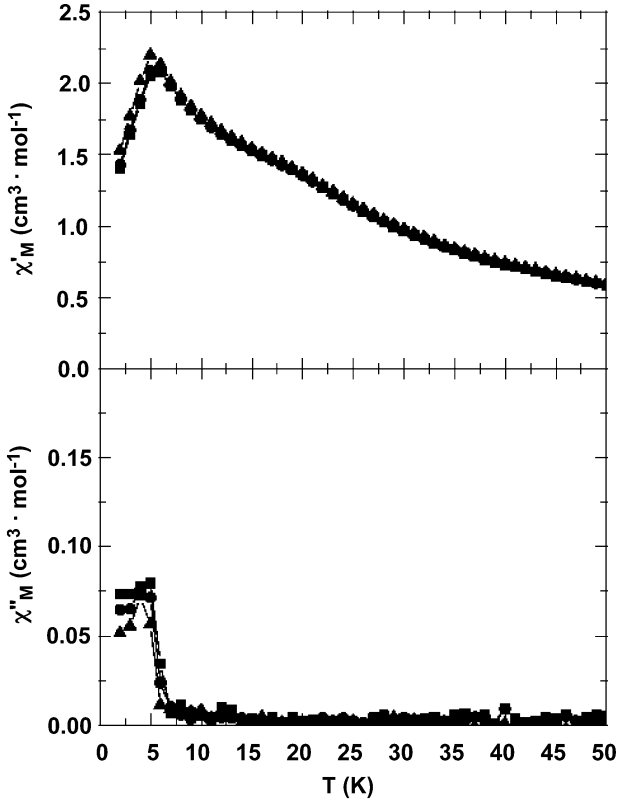

Figure 17. Plot of the molar in-phase (χ'_M) and molar out-of-phase (χ''_M) components for the *ac* susceptibility vs *T* for [Co(μ-Cl)(μ-SSi^{t}Bu$_3$)]$_{14}$ (**5**−CoCl). The measurement was performed with a 1 G field oscillating at the frequencies 1000 (squares), 500 (circles), and 50 Hz (triangles). The solid lines are meant to quide the eyes and do not represent a theoretical fit.

detailed in accordance with brief reports by Wiberg.[8] Utilization of the triflate, ^{t}Bu$_3$SiOTf,[11] and anhydrous NaSH toward thiol production is highly recommended. While timewise the reaction sequences are similar, the simplicity and high yields achieved via the triflate render the disulfide route uncompetitive. Of course, the intermediate ^{t}Bu$_3$SiSSSi^{t}Bu$_3$ may itself be useful as a reagent, but it can be generated easily upon oxidation of the thiolate.

1.2. Oligomer Precursors and [(ᵗBu₃SiS)M]₂(μ-SSiᵗBu₃)₂ (M = Fe, 1₂; Ni, 7). Precursors to the wheel and ellipse are generally very simple coordination compounds that hold few surprises. All of the metal centers are tetrahedral and linked via thiolate bridges, and while the oligomeric nature of **3**−Br and, presumably **3**−Cl, are modestly interesting, the structure of **3**−Br reveals no particular geometric feature of significance.

The most interesting small aggregates discovered during this investigation are the dimers, [(^{t}Bu$_3$SiS)M]$_2$(μ-SSi^{t}Bu$_3$)$_2$ (M = Fe, **1**$_2$; Ni, **7**). Possessing pseudo-trigonal M(II) centers, these compounds are uncommon, and the modest pyramidal distortion of each Fe in **1**$_2$, while probably steric in origin, renders its structure unique. Likewise, a literature search has not revealed other Ni(II) thiolate dimers of a pseudo-trigonal nature. Although Power and co-workers synthesized a number of three-coordinate metal dimers [(ArS)M]$_2$(μ-SAr)$_2$ (M = Mn, Fe, Co; Ar = 2,4,6-^{t}Bu$_3$C$_6$H$_2$),[14] no comparable work has been found for nickel. The reactivity and properties of these dimers will be investigated further.

1.3. Wheels and Ellipse. Lowering the coordination number through desolvation—whether in situ or via well-characterized precursors—is a reasonable approach to oligomer formation when the metal−solvent bonds are weak, as they are in these first row cases that involve THF. Modest thermolysis conditions—typically <120 °C—were quite effective in removal of THF and any remaining salt that was bound with the aid of solvent. It is unknown what the mechanism of aggregation is upon desolvation and dissolution in benzene (or hexane, as in the case of **5**−NiBr), but it is convenient to think of the oligomerization of "^{t}Bu$_3$SiSMX". As the 2-coordinate species dimerizes, then adds another segment, etc., the growing chain has two possibilities for growth: (1) one in which a helical chain is formed as the bulky μ-SSi^{t}Bu$_3$ unit moves from one bridging position to the next by ∼90° jumps until all four positions (looking down a chain) are used and the sequence is repeated indefinitely and (2) one in which the bulky μ-SSi^{t}Bu$_3$ unit alternates between two positions, causing the growing chain to bend due to growing peripheral steric influences, and ultimately generating the ring. If one accepts the premise that the wheels are unlikely to be entropically favored with respect to a distribution of oligomers, then perhaps greater relief of ^{t}Bu group steric interactions in the wheels and ellipse are at the origin of ring formation. Unfortunately, with a limited ability to characterize solution phase aggregates, the

mechanism of ring formation, and even the thermodynamics of the system, must remain the subject of speculation.

In the past 15 years, there have been numerous reports of ring or wheel compounds, yet those described herein are quite unusual in that a cyclic array of tetrahedra, bent at the M(μ-X)(μ-SSi^{t}Bu$_3$) "hinges", comprise the molecules. Most versions consist of linked octahedra containing M(III) (M = Cr,[28−31] Fe)[32−38] or M(II) (M = Mn,[39,40] Co,[41−43] Ni)[44,45] ions coordinated by "hard" oxygen- or nitrogen-based ligands, including many that are bidentate or polydentate. Excluding polyoxoanions, few rings exist in group 5[46] or in the second (e.g., β-MoCl$_4$ or [MoCl$_2$(μ-Cl)$_2$]$_6$)[47] or third rows. Some early thiolate-based rings were comprised of square planar metal centers, such as the hexamer [Ni(μ-SEt)$_2$]$_6$.[48] Related tetrameric Ni(II) thiolates,[49] pentamers[50,51] and octamers[52]—including those of Cu(II)[53,54]—are also known. It is clear that the steric bulk of ^{t}Bu$_3$SiS must play a significant role in allowing "(^{t}Bu$_3$SiS)$_2$Ni" to diimerize but not aggregate further.

In terms of rings composed of tetrahedra, there are a few for comparison. [Fe$_6$S$_6$I$_6$]$^{2-}$ is a mixed-valence iron cluster,[55] whose tetrahedra are linked via adjacent edges that utilize μ_3-S bridges connecting FeI units in a D_{3d} barrel arrangement. A spectacular ring structure based on linked tetrahedra is the mixed-valence iron−sulfur cluster [Na$_2$Fe$_{18}$S$_{30}$],$^{8-}$ in which 14 FeS$_4$ units share tetrahedral edges to form a toroid and 4 additional iron centers bind the ring to form incomplete cubes.[56] The most relevant predecessor is the dodecanuclear wheel, [Fe(μ-SePh)$_2$]$_{12}$,[57] which is the first example of the type of wheel described herein, having μ-SePh ligands that alternate above and below the ring plane.

While the wheels **5**−MX (MX = FeCl, FeBr, CoCl, NiBr) fit as a subset within the structural types mentioned above, the ellipse **6**−FeI is quite unusual, and related cyclic arrays have not been found in the literature. In fact, very few ring structures possessing greater than 12 metal centers have been noted,[33,34,40,45,56] and while [Na$_2$Fe$_{18}$S$_{30}$]$^{8-}$ is elliptical in shape, μ-sulfide bonds to counterions render it quite distinct from neutral **6**−FeI.

2. Wheel Magnetic Studies. For three cases, **5**−FeBr, **6**−FeI, and **5**−CoCl, the wheels exhibited weak antiferromagnetic behavior consistent with poorly coupled tetrahedral metal centers. Despite the apparent high symmetry of the rings, their intrinsic complexity precludes a standard analysis. The ferrous chloride **5**−FeCl manifested modest ferromagnetic coupling, and the nature of the system suggests that a spin-canting mechanism may be operational[24] since the steric shielding of the system would tend to minimalize any intermolecular interactions. Susceptibility studies that were conducted in *ac* mode revealed features of **5**−FeCl, **6**−FeI, and **5**−CoCl that pointed toward molecular magnetism.[26,27] However, the modest intensity and apparent lack of a

(28) McInnes, E. J. L.; Anson, C.; Powell, A. K.; Thomson, A. J.; Poussereau, S.; Sessoli, R. *J. Chem. Soc., Chem. Commun.* **2001**, 89−90.

(29) (a) Atkinson, I. M.; Benelli, C.; Murrie, M.; Parsons, S.; Winpenny, R. E. P. *J. Chem. Soc., Chem. Commun.* **1999**, 285−286. (b) Larsen, F. K.; Overgaard, J.; Parsons, S.; Rentschler, E.; Smith, A. A.; Timco, G. A.; Winpenny, R. E. P. *Angew. Chem., Int.* Ed. **2003**, *42*, 5978−5981. (c) Larsen, F. K.; McInnes, E. J. L.; El Mkami, H.; Rajaraman, G.; Rentschler, E.; Smith, A. A.; Smith, G. M.; Boote, V.; Jennings, M.; Timco, G. A.; Winpenny, R. E. P. *Angew. Chem., Int. Ed.* **2003**, *42*101−105.

(30) Gérbéléu, N. V.; Struchkov, Y. T.; Timco, G. A.; Batsanov, A. S.; Indrichan, K. M.; Popovich, G. A. *Dokl. Akad. Nauk. SSSR* **1990**, *313*, 1459−1462.

(31) Eshel, M.; Bino, A.; Felner, I.; Johnston, D. C.; Luban, M.; Miller, L. L. *Inorg. Chem.* **2000**, *39*, 1376−1380.

(32) (a) Taft, K. L.; Lippard, S. J. *J. Am. Chem. Soc.* **1990**, *112*, 9629−9630. (b) Taft, K. L.; Delfs, C. D.; Papaefthymiou, G. C.; Foner, S.; Gatteschi, D.; Lippard, S. J. *J. Am. Chem. Soc.* **1994**, *116*, 823−831.

(33) Watton, S. P.; Fuhrmann, P.; Pence, L. E.; Caneschi, A.; Cornia, A.; Abbati, G. L.; Lippard, S. J. *Angew. Chem., Int. Ed. Engl.* **1997**, *36*, 2774−2776.

(34) Jones, L. F.; Batsanov, A.; Brechin, E. K.; Collison, D. Helliwell, M.; Mallah, T.; McInnes, E. J. L.; Piligkos, S. *Angew. Chem., Int. Ed.* **2002**, *41*, 4318−4321.

(35) (a) Benelli, C.; Parsons, S.; Solan, G. A.; Winpenny, R. E. P. *Angew. Chem., Int. Ed. Engl.* **1996**, *35*, 1825−1828. (b) Abu-Nawwas, A. A. H.; Cano, J.; Christian, P.; Mallah, T.; Rajaraman, G.; Teat, S. J.; Winpenny, R. E. P.; Yukawa, Y. *Chem. Commun.* **2004**, 314−315.

(36) Raptopoulou, C. P.; Tangoulis, V. Devlin, E. *Angew. Chem., Int. Ed.* **2002**, *41*, 2386-2389.

(37) (a) Caneschi, A.; Cornia, A.; Fabretti, A. C.; Gatteschi, D. *Angew. Chem. Int. Ed.* **1999**, *38*, 1295−1297. (b) Abbati, G. L.; Caneschi, A.; Cornia, A.; Fabretti, A. C.; Gatteschi, D. *Inorg. Chim. Acta* **2000**, *297*, 291−300. (c) Caneschi, A.; Cornia, A.; Lippard, S. J. *Angew. Chem., Int. Ed. Engl.* **1995**, *34*, 467−469. (d) Caneschi, A.; Cornia, A.; Fabretti, A. C.; Foner, S.; Gatteschi, D.; Grandi, R.; Schenetti, L. *Chem. Eur. J.* **1996**, *2*, 1379−1387.

(38) Saalfrank, R. W.; Bernt, I.; Uller, E.; Hampel, F. *Angew. Chem., Int. Ed. Engl.* **1997**, *36*, 2482−2485.

(39) (a) Abbati, G. L.; Cornia, A.; Fabretti, A. C.; Caneschi, A.; Gatteschi, D. *Inorg. Chem.* **1998**, *37*, 1430−1431. (b) Caneschi, A.; Gatteschi, D.; Laugier, J.; Rey, P.; Sessoli, R.; Zanchini, C. *J. Am. Chem. Soc.* **1988**, *110*, 2795−2799.

(40) Liu, S.X.; Lin, S.; Lin, B.-Z.; Lin, C.-C.; Huang, J-Q. *Angew. Chem., Int. Ed.* **2001**, *40*, 1084−1087.

(41) Beattie, J. K.; Hambley, T. W.; Klepetko, J. A.; Masters, A. F.; Turner, P. *J. Chem. Soc., Chem. Commun.* **1998**, *45−46*, 14.

(42) Brechin, E. K.; Cador, O.; Caneschi, A.; Cadiou, C.; Harris, S. G.; Parsons, S.; Vonci, M.; Winpenny, R. E. P. *J. Chem. Soc., Chem. Commun*. **2002**, 1860−1861.

(43) Jones, P. L.; Byrom, K. J.; Jeffery, J. C.; McCleverty, J. A.; Ward, M. D. *J. Chem. Soc., Chem. Commun.* **1997**, 1361−1362.

(44) (a) Blake, J.; Grant, C. M.; Parsons, S.; Rawson, J. M.; Winpenny, R. E. P. *Chem. Commun.* **1994**, 2363−2364. (b) Andres, H.; Basler, R.; Blake, A. J.; Cadiou, C.; Chaboussant, G.; Grant, C. M.; Gudel, H. U.; Murrie, M.; Parsons, S.; Paulson, C.; Semadini, F.; Villar, V.; Wernsdorfer, W.; Winpenny, R. E. P. *Chem. Eur. J.* **2002**, *8*, 4867−4876.

(45) Dearden, A. L.; Parsons, S.; Winpenny, R. E. P. *Angew. Chem., Int. Ed.* **2001**, *40*, 151−154.

(46) Chen, Q.; Liu, S.; Zubieta, J. *Inorg. Chem.* **1989**, *28*, 4434−4436.

(47) Müller, U. *Angew. Chem., Int. Ed. Engl.* **1981**, *20*, 692−693.

(48) (a) Woodward, P.; Dahl, L. F.; Abel, E. W.; Crosse, B. C. *J. Am. Chem. Soc.* **1965**, *87*, 5251−5253. (b) For a Pd analogue, see: Kunchur, N. R. *Acta Crystallogr. Sect. B* **1968**, *B24*, 1623−1634.

(49) Gaete, W.; Ros, J.; Solans, X.; Font-Altaba, M.; Briansó, J. L. *Inorg. Chem.* **1984**, *23*, 39−43.

(50) Koo, B.-K.; Block, E.; Kang, H.; Liu, S.; Zubieta, J. *Polyhedron* **1988**, *7*, 1397−1399.

(51) Kriege, M.; Henkel, G. *Z. Naturforsch. B.* **1987**, *42*, 1121−1128.

(52) Dance, I. G.; Scudder, M. L.; Secomb, R. *Inorg. Chem.* **1985**, *24*, 1201−1208.

(53) Galy, J.; Mosset, A.; Grenthe, I.; Puigdomènech, I.; Sjöberg, B.; Hultén, F. *J. Am. Chem. Soc.* **1987**, *109*, 380−386.

(54) a) Ardizzoia, G. A.; Angaroni, M. A.; La Monica, G.; Cariati, F.; Moret, M.; Masciocchi, N. *J. Chem. Soc., Chem. Commun.* **1990**, 1021−1023. (b) Ardizzoia, G. A.; Angaroni, M. A.; La Monica, G.; Cariati, F.; Cenini, S.; Moret, M.; Masciocchi, N. *Inorg. Chem.* **1991**, *30*, 4347−4353.

(55) Saak, W.; Henkel, G.; Pohl, S. *Angew. Chem., Int. Ed. Engl.* **1984**, *23*, 150−151.

(56) You, J.-F.; Synder, B. S.; Papaefthymiou, G. C.; Holm, R. H. *J. Am. Chem. Soc.* **1990**, *112*, 1067−1076.

(57) Fenske, D.; Fischer, A. *Angew. Chem., Int. Ed. Engl.* **1995**, *34*, 307−309.

frequency dependence in the out-of-phase measurements have effectively ruled this out. At the low temperatures the phenomena were observed, the compounds were likely undergoing phase changes

The study and synthesis of antiferromagnetic rings has been pointed out as a significant area of research for nanomagnetism in a recent review.[58] The quantum effects associated with these antiferromagnetic rings are expected to be important. Quantum coherence is achieved when a material can tunnel (or "oscillate") between two states without dissipating or absorbing energy from its environment. A necessary precondition for quantum computing[59] with electronic spin states is their coherent evolution under controlled perturbations. The electronic spins in molecular magnets interact with their environment, which includes nuclear spins, lattice vibrations, and other molecular magnets in the crystal. These tend to destroy the coherence and, for example, reduce the expected quantum oscillations between "up" and "down" spin states to an "incoherent" tunneling transition between these states. The quantum tunneling in an antiferromagnetic ring is predicted to occur coherently.[60,61] If there are an odd number of antiferromagnetically coupled spin carriers in a ring, the compound will have an uncompensated spin ground state.[62] For example, a compound with thirteen antiferromagnetically coupled $S = {}^1/_2$ spin carriers will have a spin ground state of $S = {}^1/_2$. If the remaining uncompensated spin ($S = {}^1/_2$ in this case) is forced to change orientations from a "spin-up" to a "spin-down" ($m_s = -{}^1/_2$ to $m_s = {}^1/_2$) then all the other spin carriers in the ring must also reverse their spin in order to maintain the antiferromagnetic exchange interaction. At low enough temperatures, this is expected to occur by a tunneling mechanism and also to occur coherently. One can also still observe quantum effects in even-numbered antiferromagnetic rings. If there is a low-lying excited spin-state not far in energy from the $S = 0$ ground state, one can populate this excited state by applying a strong magnetic field. At high enough magnetic field, the excited state will cross over and become lower in energy than the ground state. At low enough temperatures, this crossover can occur via quantum tunneling. Gatteschi and Lippard et al. have examined this for an Fe_{10} "ferric wheel".[32] At certain intervals of applied magnetic field, crossovers were observed from the ground state to low-lying excited states. The cobalt wheel **5**−CoCl was examined in a similar way (Figure 18), and an essentially linear response of $M/\beta N$ vs H is observed. This is typical for an antiferromagnet, and no crossover was observed. It is likely that the required magnetic field to induce a crossover is much higher than the instrumentation utilized.

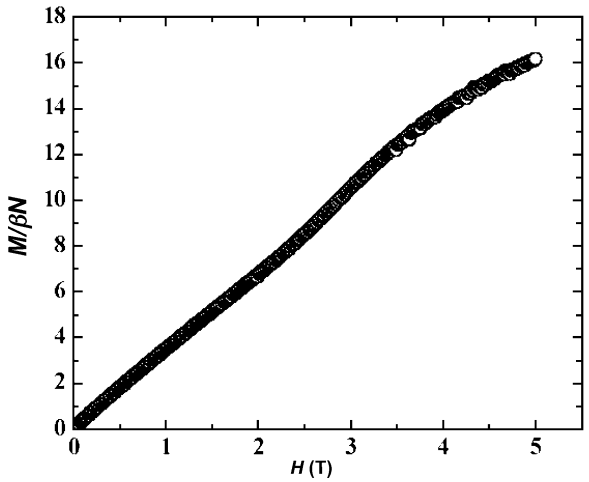

Figure 18. Plot of the reduced magnetization ($M/\beta N$), where M is the molar magnetization, N is Avogadro's number, and β is the Bohr magneton, vs H (in Tesla) for $[Co(\mu\text{-}Cl)(\mu\text{-}SSi^tBu_3)]_{14}$ (**5**−CoCl). The data were collected at 5.0 K.

In summary, only modest couplings—both antiferromagnetic and ferromagnetic—were observed for the wheels and ellipse, presumably due to rather long intermetallic distances. No further investigations were conducted.

Experimental Section

1. General Considerations. All manipulations were performed using either glovebox or high-vacuum-line techniques. Hydrocarbon solvents containing 1−2 mL of added tetraglyme and ethereal solvents were distilled under nitrogen from purple sodium benzophenone ketyl and vacuum-transferred from the same prior to use. C_6D_6 was dried over activated 4 Å molecular sieves, vacuum-transferred, and stored under N_2. The compounds $^tBu_3SiNa(THF)_2$,[10] $^tBu_3SiOTf$,[11,63] $FeCl_2(THF)_2$,[64] $FeBr_2(THF)_2$,[65] $FeI_2(THF)_2$,[65] and $NiBr_2(THF)_2$[66] were prepared according to literature procedures. All glassware was oven-dried, and NMR tubes for sealed tube experiments were additionally flame-dried under dynamic vacuum.

NMR spectra were obtained using INOVA-400 and Unity-500 spectrometers, and chemical shifts are reported relative to C_6D_6 (^1H, 7.15; $^{13}C\{^1H\}$, 128.39) and THF-d_8 (^1H, 1.73; $^{13}C\{^1H\}$, 25.37). Infrared spectra were recorded on a Nicolet Impact 410 spectrophotometer interfaced to a Gateway PC. Elemental analyses were performed by Oneida Research Services, Whitesboro, NY, or Robertson Microlit Laboratories, Madison, NJ. Magnetic moments were determined in C_6D_6 or THF-d_8 at room temperature using Evans' method[16] with an applied diamagnetic correction.

2. Procedures. 2.1. $^tBu_3SiS-SSi^tBu_3$. A solution of S_2Cl_2 (1.24 mL, 15.50 mmol, ∼10 mL THF) was added dropwise to a solution of $^tBu_3SiNa(THF)_{2.6}$ (12.15 g, 29.64 mmol, ∼50 mL THF) cooled to 0 °C. After addition was complete, the solution was allowed to warm to 23 °C and stirred for 4.5 h. The solvent was removed in vacuo, and the residue was extracted into pentane and filtered through Celite. Solid product was obtained by cooling a concentrated pentane solution to −78 °C to afford 5.06 g of $^tBu_3SiS-SSi^tBu_3$ (74% yield). ^1H NMR (C_6D_6): δ 1.31 (s, CH_3). $^{13}C\{^1H\}$

(58) Gatteschi, D.; Sessoli, R. *Angew. Chem., Int. Ed.* **2003**, *42*, 268−297.
(59) (a) Leuenberger, M. N.; Loss, D. *Nature* **2001**, *410*, 789−793. (b) DiVincenzo, D. P.; Loss, D. *J. Magn. Magn. Mater.* **1999**, *200*, 202−218.
(60) Meier, F.; Loss, D. *Physica B: Condens. Matt.* **2003**, *329*, 1140−1141.
(61) Troiani, F.; Ghirri, A.; Affronte, M.; Carretta, S.; Santini, P.; Amoretti, G.; Piligkos, S.; Timco, G.; Winpenny, R. E. P. *Phys. Rev. Lett.* **2005**, *94*, 207−208.
(62) Bartlett, B. M.; Nocera, D. G. *J. Am. Chem. Soc.* **2005**, *127*, 8985−8993.
(63) Eaborn, C.; Saxena, A. K. *J. Organomet. Chem.* **1984**, *271*, 33−46.
(64) Herzog, S.; Gustav, K.; Kruger, E.; Oberender, H.; Schuster, R. *Z. Chem.* **1963**, *3*, 428−429.
(65) Ittel, S. D.; English, A. D.; Tolman, C. A.; Jesson, J. P. *Inorg. Chim. Acta* **1979**, *33*, 101−106.
(66) Casalnuovo, A. L.; RajanBabu, T. V.; Ayers, T. A.; Warren, T. H. *J. Am. Chem. Soc.* **1994**, *116*, 9869−9882.

NMR (C_6D_6): δ 26.36 ($C(CH_3)_3$), 31.18 ($C(CH_3)_3$). Anal. Calcd for $C_{12}H_{27}SiS$: C, 62.2; H, 11.8. Found: C, 61.7; H, 11.3.

2.2. ^{t}Bu$_3$SiSH. 2.2.1. Substitution of ^{t}Bu$_3$SiOTf. A 25 mL round-bottom flask attached to a reflux condenser was charged with ^{t}Bu$_3$SiOTf (1.00 g, 2.869 mmol), anhydrous NaSH (0.161 g, 2.872 mmol), and THF (10 mL). The solution was refluxed under argon for 3 d, and the solvent was removed in vacuo. The solid was then extracted with pentane, and the solution was filtered, stripped of solvent, and sublimed to give ^{t}Bu$_3$SiSH (0.561 g, 84%). ^{1}H NMR (C_6D_6): δ −0.57 (s, 1H, SH), 1.10 (s, 27H, CH_3). ^{13}C{^{1}H} NMR (C_6D_6): δ 24.14 ($C(CH_3)_3$), 30.66 ($C(CH_3)_3$). IR (Nujol Mull, NaCl, cm^{-1}): 2178 (w), 1303 (w), 1192 (m), 1014 (m), 932 (m), 817 (s), 608 (m), 578 (m), 522 (m), 456 (m). Anal. Calcd for $C_{13}H_{27}SiS$: C, 62.0; H, 11.7. Found: C, 62.2; H, 12.2.

2.2.2. LiAlH$_4$ Reduction of ^{t}Bu$_3$SiS−SSi^{t}Bu$_3$. A heterogeneous mixture of ^{t}Bu$_3$SiS−SSi^{t}Bu$_3$ (2.60 g, 5.615 mmol) and $LiAlH_4$ (1.50 g, 39.52 mmol) in THF (60 mL) was refluxed under argon for 2 d. The excess $LiAlH_4$ was deactivated by H_2O addition at 0 °C, and the solution was acidified with aqueous 5 M HCl. The THF was removed in vacuo and the product was extracted with Et_2O and dried over $MgSO_4$. Solvent removal followed by sublimation gave 2.18 g of crystalline ^{t}Bu$_3$SiSH in 84% yield.

2.2.3. Protonation of ^{t}Bu$_3$SiSNa(THF)$_x$. A 50 mL flask was charged with ^{t}Bu$_3$SiSNa(THF)$_{1.9}$ (3.043 g, 7.77 mmol) and attached to a gas bulb. THF (20 mL) was added at −78 °C and the flask was cooled to 77 K. HCl (538 Torr in 265.8 mL, 7.77 mmol) was condensed into the flask, and the solution was slowly warmed to 23 °C. After the mixture was stirred for 30 min, the volatiles were stripped and the solid was triturated three times with hexanes. The crude solid was dissolved in hexane and filtered through a pad of Celite. Volatiles were removed in vacuo to yield 1.52 g of crystalline ^{t}Bu$_3$SiSH (84% yield).

2.3. ^{t}Bu$_3$SiSNa(THF)$_x$ (x = 1.4−1.9). 2.3.1. Sodium Reduction of ^{t}Bu$_3$SiSH. A 100 mL round-bottom flask was charged with ^{t}Bu$_3$SiSH (2.40 g, 10.3 mmol), sodium metal (0.48 g, 20.9 mmol), and THF (50 mL). The mixture was stirred overnight, filtered, concentrated, crystallized at −78 °C, and dried in vacuo to afford white, crystalline ^{t}Bu$_3$SiSNa(THF)$_{1.40}$ (3.37 g, 92%). ^{1}H NMR (C_6D_6): δ 1.36 (s, 27 H, CH_3), 1.41 (m, 4H, OCH_2CH_2), 3.61 (t, 4H, OCH_2CH_2). ^{13}C{^{1}H} NMR (C_6D_6): δ 25.83 ($C(CH_3)_3$), 32.07 ($C(CH_3)_3$). IR (Nujol Mull, NaCl, cm^{-1}): 1180 (m), 1050 (m), 1013 (m), 932 (w), 912 (w), 817 (m), 603 (m), 588 (m), 529 (m), 461 (m). Anal. Calcd for $C_{16}H_{35}ONaSiS$ (desolvated): C, 58.8; H, 10.8. Found: C, 58.6; H, 10.9.

2.3.2. Na/Hg Reduction of ^{t}Bu$_3$SiS−SSi^{t}Bu$_3$. A 100 mL round-bottom flask was charged with ^{t}Bu$_3$SiS−SSi^{t}Bu$_3$ (1.42 g, 3.07 mmol), freshly made 0.9% Na/Hg amalgam (30.3 g, 11.9 mmol Na°), and THF (60 mL). The heterogeneous mixture was stirred for 3 days, filtered, and concentrated at −78 °C yielding ^{t}Bu$_3$SiSNa(THF)$_{1.90}$ (1.32 g, 55%).

2.4. [(^{t}Bu$_3$SiS)Fe]$_2$(μ-SSi^{t}Bu$_3$)$_2$ (1$_2$). A 50 mL flask was charged with [{$(Me_3Si)_2N$}$_2$Fe]$_2$ (1.099 g, 2.918 mmol), ^{t}Bu$_3$SiSH (1.357 g, 5.836 mmol), and 25 mL of benzene at 23 °C. Upon being stirred for 30 min, the volatiles were removed and the brown solid was subjected to dynamic vacuum for 3 h. The material was dissolved in pentane, filtered, and cooled to −78 °C to provide 1.308 g of orange **1**$_2$ (86%). ^{1}H NMR (C_6D_6, 23 °C): δ 1.91 ($\nu_{1/2}$ = 200 Hz), 3.63 ($\nu_{1/2}$ = 200 Hz). Anal. Calcd for $C_{24}H_{54}Si_2S_2Fe$: C, 55.56; H, 10.49. Found: C, 55.3; H, 10.6.

2.5. (^{t}Bu$_3$SiS)$_2$Fe(THF)$_2$ (1−(THF)$_2$). A 25 mL flask was charged with **1**$_2$ (200 mg, 0.193 mmol) and 15 mL of THF at −78 °C. The solution was slowly brought to 23 °C, and the THF was removed. Pentane (∼15 mL) was added, and the solution was filtered and cooled to −78 °C to yield 118 mg of **1**−(THF)$_2$ (46%). ^{1}H NMR (C_6D_6): δ 2.84 ($\nu_{1/2} \approx$ 40 Hz, CH_3), 1.87 ($\nu_{1/2} \approx$ 30 Hz, OCH_2CH_2), 4.68 ($\nu_{1/2} \approx$ 80 Hz, OCH_2CH_2).

2.6. (^{t}Bu$_3$SiS)$_3$Fe(THF) (1−(THF)$_2$). A 25 mL flask was charged with 0.250 g (0.692 mmol) of NaSSi^{t}Bu$_3$(THF)$_{1.48}$, 37 mg of $FeCl_3$ (0.23 mmol), and 15 mL of THF at −78 °C. The reaction mixture was allowed to slowly warm to 23 °C over the course of 8 h and was stirred for 1 h at 23 °C. The THF was removed, and the solid was triturated with pentane (3 × 5 mL). Pentane (∼15 mL) was added, and the mixture was filtered and washed. The solution was filtered, the salt cake was washed (3 × 2 mL) with pentane, and the extracts were reduced to ∼5 mL and cooled to −78 °C to produce purple crystals of **2**−THF (190 mg, 85%). ^{1}H NMR (C_6D_6): δ 21.4 ($\nu_{1/2} \approx$ 1100 Hz). The compound was too thermally sensitive to submit for analysis.

2.7. [Cl$_2$Fe](μ-SSi^{t}Bu$_3$)$_2$[FeCl(THF)]Na(THF)$_4$ (3−Cl). A 50 mL flask was charged with NaSSi^{t}Bu$_3$(THF)$_{1.48}$ (0.250 g, 0.692 mmol), $FeCl_2(THF)_2$ (0.188 g, 0.694 mmol), and THF (20 mL). The pale yellow solution was stirred for 18 h, filtered, and the solvent allowed to slowly evaporate to give crystalline **3**−Cl (0.271 g, 74%). ^{1}H NMR (THF-d_8): δ 9.11 ($\upsilon_{1/2} \approx$ 940 Hz). IR (Nujol Mull, NaCl, cm^{-1}): 1248 (w), 1192 (m), 1176 (m), 1018 (s), 932 (m), 915 (m), 868 (s), 817 (s), 724 (m), 679 (m), 613 (s), 570 (s), 515 (s), 460 (s), 423 (m). Anal. Calcd $C_{28}H_{62}OSi_2S_2NaCl_3Fe_2$ (desolvated): C, 43.3; H, 8.1; Cl, 13.7. Found: C, 42.5; H, 8.2; Cl, 13.4. μ_{eff} = 4.8 μ_B at 295 K (Evans' method in THF-d_8). A quench with DCl/CD_3OD afforded thiolate/THF = 1.0:3.9 by ^{1}H NMR spectroscopic analysis.

2.8. [Br$_2$Fe](μ-SSi^{t}Bu$_3$)$_2$[FeBr(THF)]Na(THF)$_4$ (3−Br). A 50 mL flask was charged with NaSSi^{t}Bu$_3$(THF)$_{1.68}$ (0.325 g, 0.865 mmol), $FeBr_2(THF)_2$ (0.311 g, 0.864 mmol), and THF (20 mL). The pale yellow solution was stirred for 18 h, filtered, and the solvent allowed to slowly evaporate to give 0.446 g **3**−Br (86%). ^{1}H NMR (THF-d_8): δ 12.46 ($\upsilon_{1/2} \approx$ 280 Hz). IR (Nujol Mull, NaCl, cm^{-1}): 1260 (m), 1180 (m), 1057 (s), 1014 (s), 934 (m), 915 (m), 858 (s), 817 (s), 722 (w), 613 (s), 574 (s), 515 (s), 462 (s). Anal. Calcd $C_{32}H_{70}O_2Si_2S_2Na\ Br_3Fe_2$ (desolvated): C, 42.7; H, 7.9; Br, 21.3. Found: C 42.3, H 7.9, Br 21.8. μ_{eff} = 4.5 μ_B at 295 K (Evans method in THF-d_8). A quench with DCl/CD_3OD afforded thiolate/THF = 1.0:3.9 by ^{1}H NMR spectroscopic analysis.

2.9. *cis*-[(THF)IFe]$_2$(μ-SSi^{t}Bu$_3$)$_2$ (4). A 50 mL flask was charged with NaSSi^{t}Bu$_3$(THF)$_{1.68}$ (0.504 g, 1.34 mmol), $FeI_2(THF)_2$ (0.608 g, 1.34 mmol), and THF (25 mL). The yellow solution was stirred for 24 h, filtered, and the solvent was removed. The yellow solid was heated under vacuum at 98 °C for 2 h, extracted into benzene (40 mL), and filtered. Slow evaporation of the solvent afforded **4** (0.485 g, 75%) after 5 days. ^{1}H NMR (C_6D_6): δ 6.82 ($\upsilon_{1/2} \approx$ 140 Hz). IR (Nujol Mull, NaCl, cm^{-1}): 1243 (w), 1188 (m), 1176 (m), 1014 (s), 934 (s), 858 (s), 817 (s), 724 (w), 677 (m), 615 (s), 566 (s). Anal. Calcd $C_{12}H_{27}SiSIFe$ (desolvated): C, 34.8; H, 6.6; I, 30.6. Found: C, 33.4; H, 6.4; I, 27.7. μ_{eff}/Fe = 4.8 μ_B at 295 K (Evans' method in C_6D_6). A quench with DCl/CD_3OD afforded thiolate/THF = 1.0:0.9 by ^{1}H NMR spectroscopic analysis.

2.10. [Fe(μ-Cl)(μ-SSi^{t}Bu$_3$)]$_{12}$(C_6H_6)$_7$ (5−FeCl). A 50 mL flask was charged with **3**−Cl (0.271 g, 0.255 mmol) and heated under vacuum at 80 °C for 1.5 h. The product was extracted with benzene and filtered, and yellow crystalline **5**−FeCl (0.082 g, 45%) deposited after slow evaporation of the solvent (6 d). IR (Nujol Mull, NaCl, cm^{-1}): 1192 (m), 1178 (m), 1014 (s), 981 (m), 934 (s), 872 (w), 817 (s), 724 (w), 677 (s), 615 (s), 566 (s). Anal. Calcd $C_{12}H_{27}SiSClFe$ (desolvated): C, 44.6; H, 8.5; Cl, 11.0. Found: C, 43.9; H, 8.4; Cl, 9.9. A quench with DCl/CD_3OD afforded thiolate/C_6H_6 = 1.0:0.6 by ^{1}H NMR spectroscopic analysis.

2.11. [Fe(μ-Br)(μ-SSiᵗBu₃)]₁₂(C₆H₆)₁₂ (5−FeBr). A 100 mL flask was charged with $NaSSi^tBu_3(THF)_{1.40}$ (0.801 g, 2.25 mmol), $FeBr_2(THF)_2$ (0.736 g, 2.28 mmol), and THF (50 mL). The mixture was stirred at 23 °C for 24 h, and the solvent was removed to yield a yellow solid. The solid was heated at 79 °C under vacuum for 2 h then extracted into benzene and filtered. After slow evaporation of the solvent (5 days), yellow crystals of **5**−FeBr formed (0.739 g, 72%). ^{1}H NMR (C_6D_6): δ 4.84 ($\upsilon_{1/2} \approx 60$ Hz, tentative). IR (Nujol Mull, NaCl, cm^{-1}): 1190 (s), 1180 (s), 934 (s), 817 (s), 726 (w), 675 (s), 615 (s), 568 (s), 501 (s), 462 (s). Anal. Calcd $C_{12}H_{27}SiSBrFe$ (desolvated): C, 39.2; H, 7.4; Br, 21.8. Found: C, 39.7; H, 7.3; Br, 21.8. A quench with DCl/CD_3OD afforded thiolate/C_6H_6 = 1.0:1.0 by ^{1}H NMR spectroscopic analysis.

2.12. [Fe(μ-I)(μ-SSiᵗBu₃)]₁₄(C₆H₆)₁₄ (6−FeI). A 50 mL flask was charged with $NaSSi^tBu_3(THF)_{1.56}$ (0.301 g, 0.820 mmol), $FeI_2(THF)_2$ (0.371 g, 0.817 mmol), and THF (20 mL). The mixture was stirred at 23 °C for 24 h, and the solvent was removed to yield a yellow solid. The solid was heated at 117 °C under vacuum for 5 h then extracted into benzene and filtered. After slow evaporation of the solvent (7 days), dark yellow crystals formed (0.064 g, 16%). ^{1}H NMR (C_6D_6): insoluble. IR (Nujol Mull, NaCl, cm^{-1}): 1190 (s), 1180 (s), 1012 (s), 936 (s), 860 (w), 815 (s), 726 (w), 675 (m), 615 (s), 566 (s), 492 (s), 462 (s). Anal. Calcd $C_{12}H_{27}SiSIFe$ (desolvated): C, 34.8; H, 6.6; I, 30.6. Found: C, 28.8; H, 5.2; I, 30.3. A quench with DCl/CD_3OD afforded thiolate/C_6H_6 = 1.0:0.9 by ^{1}H NMR spectroscopic analysis.

2.13. [Co(μ-Cl)(μ-SSiᵗBu₃)]₁₂(C₆H₆)₆ (5−CoCl). A 100 mL flask was charged with $CoCl_2$ (0.347 g, 2.673 mmol), $NaSSi^tBu_3(THF)_{1.66}$ (1.003 g, 2.680 mmol), and THF (60 mL). The mixture was stirred at room temperature for 12 h, and the solvent was removed under vacuum. The blue solid was heated at 81°C under vacuum for 1.5 h to give a green solid that was extracted into benzene and filtered. Slow evaporation of the benzene yielded the product as green microcrystals (0.206 g, 21%). ^{1}H NMR (C_6D_6): δ 9.11 ($\upsilon_{1/2} \approx 50$ Hz). IR (Nujol Mull): 1189 (m), 1013 (s), 934 (m), 816 (s), 675 (m), 614 (s), 563 (s) cm^{-1}. Anal. Calcd for $C_{12}H_{27}SiSClCo$ (desolvated): C, 44.2; H, 8.4; Cl, 10.9. Found: C, 44.2; H, 8.4; Cl, 10.9. A quench with DCl/CD_3OD afforded thiolate/benzene = 1.0:0.5 by ^{1}H NMR spectroscopic analysis.

2.14. [(ᵗBu₃SiS)Ni]₂(μ-SSiᵗBu₃)₂ (7). A 25 mL flask was charged with $NiBr_2(THF)_2$ (0.100 g, 0.276 mmol), $NaSSi^tBu_3(THF)_{1.54}$ (0.200 g, 0.547 mmol), and THF (20 mL). The mixture was stirred at 23 °C for 24 h, and the solvent was removed under vacuum. The purple solid was extracted with diethyl ether and filtered. The solution was concentrated and crystallized at −78 °C to yield the product as purple microcrystals (0.091 g, 63%). ^{1}H NMR (C_6D_6): δ 1.31 (54 H, −SSi(C(CH$_3$)$_3$)$_3$), 1.35 (54 H−SSi(C(CH$_3$)$_3$)$_3$). ^{13}C-{^{1}H} NMR (C_6D_6): δ 25.84 (*C*(CH$_3$)$_3$), 26.41 (*C*(CH$_3$)$_3$), 31.97 (C(*C*H$_3$)$_3$), 32.25 (C(*C*H$_3$)$_3$). IR (Nujol Mull): 1182 (m), 1012 (m), 934 (m), 815 (s), 611 (s), 563 (s) cm^{-1}. Anal. Calcd for $C_{24}H_{54}Si_2S_2Ni$: C, 55.2; H, 10.5. Found: C, 54.9; H, 10.9. M_w (Signer isopiestic method; solvent = pentane, standard = ferrocene) calcd: 1044, found: 1030 ± 60 (3 trials).

2.15. [Ni(μ-Br)(μ-SSiᵗBu₃)]₁₂(C₆H₁₄)ₙ (5−NiBr). A 25 mL flask was charged with $NiBr_2(THF)_2$ (0.150 g, 0.414 mmol), $NaSSi^tBu_3(THF)_{1.54}$ (0.150 g, 0.410 mmol), and THF (20 mL). The mixture was stirred at 23 °C for 16 h, and the solvent was removed under vacuum. The green solid was heated at 88 °C under vacuum for 3 h, yielding a red-purple solid that was washed with diethyl ether to remove **7** via disproportionation. The resulting green solid was extracted with hexane and filtered. Slow evaporation of the hexane over 12 h yielded the product as a microcrystalline red solid (0.026 g, 17% based on desolvated **5**−NiBr). ^{1}H NMR (C_6D_{12}): insoluble. IR(Nujol Mull): 1189 (w), 1012 (m), 934 (m), 816 (m), 614 (s), 563 (s) cm^{-1}. Anal. Calcd for $C_{12}H_{27}SiSBrNi$ (desolvated): C, 38.9; H, 7.4. Found: C, 33.5; H, 7.4.

3. Magnetic Susceptibility Measurements. Magnetic susceptibility measurements were performed on Quantum Design magnetometers. Direct current (dc) susceptibilities were collected on a model MPMS-5 SQUID magnetometer equipped with a 5.5 T magnet. Alternating current (ac) susceptibilities were collected on a model MPMS2 SQUID magnetometer. Both instruments operate in the 2−400 K temperature range. All sample preparations and manipulations were performed under an inert atmosphere to ensure that the integrities of the air-sensitive samples were preserved. The samples were either measured in a flame-sealed NMR tube or a custom-machined, sealed Teflon capsule. Variable-temperature dc susceptibility measurements were performed with an applied field of 1 T. Variable-temperature ac susceptibility measurements were performed with an oscillating ac field of 1 G and zero applied dc field. The diamagnetic contribution from the sample container was subtracted from the experimental data. Pascal's constants[24] were also used to subtract the diamagnetic contributions, yielding paramagnetic susceptibilities.

4. X-Ray Crystal Structure Determinations. 4.1. General. The selected crystal (for 173 K data collection, it was immersed in polyisobutylene) was placed in the goniometer head of a diffractometer equipped with a fine-focus molybdenum X-ray tube and graphite monochromator. Preliminary diffraction data revealed the crystal system (Tables 1 and 3), and a hemisphere routine was used to collect the data. Precise lattice constants were determined from a least-squares fit of 15 diffractometer-measured 2θ values. The space group was determined, and after correction for Lorentz, polarization, and background effects, unique data were judged observed according to $|F_o| > 2\sigma|F_o|$. All heavy atoms were located using direct methods, and all non-hydrogen atoms were revealed by successive Fourier syntheses. Full matrix, least squares refinements (minimization of $\Sigma w(F_o - F_c)^2$ where w is based on counting statistics modified by an ignorance factor, w^{-1}) with anisotropic heavy atoms and all hydrogens included at calculated positions led to the final model. Crystallographic data (CIF files) for certain structures have been deposited with the Cambridge Crystallographic Data Centre as supplementary publication nos. CCDC-203239 (**5**−FeCl), CCDC-203238 (**5**−FeBr), CCDC-203240 (**6**−FeI), CCDC-220005 (**5**−CoCl), and CCDC-220006 (**5**−NiBr). Copies of the data can be obtained free of charge on application to CCDC, 12 Union Road, Cambridge CB2 1EZ, UK (fax: (+44) 1223−336−033; E-mail: deposit @ccdc.cam.ac.uk).

4.2. [(ᵗBu₃SiS)Fe]₂(μ-SSiᵗBu₃)₂ (1₂). An orange block (0.6 × 0.5 × 0.4 mm^3) from pentane was used. Data collection on a Siemens P4 diffractometer gave 4008 of the 4940 unique data points (81.13%, $R_{int} = 0.0654$) where $|F_o| > 2\sigma|F_o|$. Refinement utilized SHELXTL PLUS and $w^{-1} = \sigma^2(F_o^2) + (0.1072p)^2 + 4.0995p$, where $p = (F_o^2 + 2F_c^2)/3$).

4.3. (ᵗBu₃SiS)₂Fe(THF)₂ (1−(THF)₂). A yellow block (0.4 × 0.3 × 0.2 mm^3) from pentane was selected. Data collection on a Siemens P4 diffractometer revealed 5733 of the 6047 unique data points (94.81%, $R_{int} = 0.0271$) where $|F_o| > 2\sigma|F_o|$. Refinement utilized SHELXTL PLUS and $w^{-1} = \sigma^2(F_o^2) + (0.0855p)^2 + 1.4794p$, where $p = (F_o^2 + 2F_c^2)/3$).

4.4. [Br₂Fe](μ-SSiᵗBu₃)₂[FeBr(THF)]Na(THF)₄ (3−Br). A yellow block (0.4 × 0.3 × 0.2 mm^3) obtained from THF was used. Data collected on a Siemens SMART CCD Area Detector system were processed with the Bruker SAINT program (17 443 reflections, 6841 were symmetry independent, $R_{int} = 0.0542$). The data were corrected for absorption with SADABS and refined using SHELX-

TL. Both of the ^{t}Bu$_3$Si groups exhibited rotational disorder around the Si−S axis, which was modeled by refining the occupancy (50%) of two sets of ^{t}Bu$_3$Si groups. The model did not refine well, but no better one was found.

4.5. *cis*-[(THF)IFe]$_2$(μ-SSi^{t}Bu$_3$)$_2$ (4). A yellow block (0.2 × 0.2 × 0.15 mm^3) was obtained from C_6H_6. Data collected on a Siemens SMART CCD Area Detector system were processed with the Bruker SAINT+ program (19 236 reflections, 6142 were symmetry independent, R_{int} = 0.0263). Refinement utilized SHELXTL.

4.6. [Fe(μ-Cl)(μ-SSi^{t}Bu$_3$)]$_{12}$(C$_6$H$_6$)$_7$ (5−FeCl). A yellow crystal (0.2 × 0.15 × 0.05 mm^3) was obtained from benzene. Data collected on a Siemens SMART CCD Area Detector system were processed with the Bruker SMART program (46 598 reflections, 9453 were symmetry independent, R_{int} = 0.0726). The data were corrected for absorption with SADABS and refined using SHELXTL. All non-hydrogen atoms were refined with anisotropic displacement parameters, except for half a benzene ring lying on a special position, and hydrogen atoms were included at calculated positions. Two and a half benzene molecules were found in the asymmetric unit. Data refinement indicated partial occupancy of the benzene sites, but independent refinement of the benzene occupancies did not yield a ^{t}Bu$_3$SiS/C$_6$H$_6$ ratio (1:0.2) consistent with the experimentally determined value of 1:0.6. The occupancy values were set to 75% for the two benzene molecules and 50% for the half benzene molecule to correspond exactly to the experimental value.

4.7. [Co(μ-Cl)(μ-SSi^{t}Bu$_3$)]$_{12}$(C$_6$H$_6$)$_6$ (5−CoCl). A green block crystal (0.3 × 0.2 × 0.15 mm^3) was obtained from benzene. Data collected on a Siemens SMART CCD Area Detector system were processed with the Bruker SAINT program (48 983 reflections, 8000 were symmetry independent, R_{int} = 0.1040). The data were corrected for absorption with SADABS and refined using SHELXTL. Two and a half benzene molecules were found in the asymmetric unit. Data refinement indicated partial occupancy of the benzene sites. The benzene occupancies were refined independently, with the two benzene occupancies refining to 68 and 71%, while the occupancy of the half-benzene refined to 46%. These values gave a ^{t}Bu$_3$SiS/C$_6$H$_6$ ratio (1:0.54) very close to that obtained by experimental methods (1:0.5), so the occupancy values were set to 62.5% for the two benzene molecules and 50% for the half benzene molecule to correspond exactly to the experimental value.

4.8. [Fe(μ-Br)(μ-SSi^{t}Bu$_3$)]$_{12}$(C$_6$H$_6$)$_{12}$ (5−FeBr). A yellow crystal (0.3 × 0.2 × 0.05 mm^3) was obtained from benzene. Data collected on a Siemens SMART CCD Area Detector system were processed with the Bruker SAINT+ program (17 324 reflections, 5190 were symmetry independent, R_{int} = 0.0976). The data were corrected for absorption with SADABS and refined using SHELXTL. The carbon atoms were not refined anisotropically due to disorder that could not be incorporated into the model due to poor data quality. The unit cell had two cavities containing a large amount of severely disordered benzene molecules. The difference Fourier map in this region showed a number of peaks, but no consistent model could be assembled. This part of the structure was modeled using the SQUEEZE procedure of the PLATON program.[19] Two symmetry-equivalent cavities centered at (0, 0, 0) and (1/2, 1/2, 0) with volumes of 2052 Å^3 (cell volume = 13 349(6) Å^3) were each occupied by 805 electrons. Since the crystallization was carried out in benzene solution, the asymmetric unit could contain, on average, 4.8 benzene molecules. The final model consisted of the ordered part only, without the disordered solvent contribution, and was refined against new data provided with the fcf file.

4.9. [Ni(μ-Br)(μ-SSi^{t}Bu$_3$)]$_{12}$(C$_6$H$_{14}$)$_n$ (5−NiBr). A red block crystal (0.5 × 0.6 × 0.6 mm^3) was obtained from pentane. Data collected on a Siemens SMART CCD Area Detector system were processed with the Bruker SAINT program (9646 reflections, 3730 were symmetry independent, R_{int} = 0.1259). The data were corrected for absorption with SADABS and refined using SHELXTL. The carbon atoms were not refined anisotropically due to disorder that could not be incorporated into the model due to poor data quality. Constraints were applied to the geometries of the ^{t}Bu$_3$Si fragments on each ^{t}Bu$_3$SiS ligand such that chemically equivalent inter- and intra-atomic distances were constrained to equal the same least-squares variables (e.g., all *d*(SiC) are equivalent; all *d*(CC) are equivalent, etc.). The unit cell had two cavities containing a large amount of severely disordered solvent molecules. The difference Fourier map in this region showed a number of peaks, but no consistent model could be assembled. This part of the structure was modeled using the SQUEEZE procedure of the PLATON program.[19] Two cavities (per cell) of 3012 Å^3 (cell volume = 14 597 Å^3) were each occupied by 464 electrons. The final model consisted of the ordered part only, without the disordered solvent contribution, and was refined against new data provided with the fcf file.

4.10. [Fe(μ-I)(μ-SSi^{t}Bu$_3$)]$_{14}$(C$_6$H$_6$)$_{14}$ (6−FeI). A yellow crystal (0.5 × 0.4 × 0.2 mm^3) was obtained from benzene. Data collected on a Siemens SMART CCD Area Detector system were processed with the Bruker SAINT+ program (104 844 reflections, 10 375 were symmetry independent, R_{int} = 0.0961). Refinement utilized SHELXTL but the carbon and silicon atoms were refined isotropically due to disorder that could not be incorporated into the model due to poor data quality. The unit cell had cavities containing a large amount of severely disordered benzene molecules. One ordered benzene was located in the center of the ring, a partially disordered benzene was located outside the ring, and several completely disordered benzenes could not be modeled. This part of the structure was modeled using the SQUEEZE procedure of the PLATON program.[19] The final model consisted of the ordered part only, without the disordered solvent contribution, and was refined against new data provided with the fcf file.

Acknowledgment. We thank the National Science Foundation (CHE-9528914 (P.T.W.)) and Cornell University for financial support.

Supporting Information Available: CIF files for **1**$_2$, **1**−(THF)$_2$, **3**−Br, and **4**. This material is available free of charge via the Internet at http://pubs.acs.org.

IC051289U